2013

Background and Available Potential Energy in Numerical Simulations of a Boussinesq Fluid

Shreyas S. Panse
University of Massachusetts Amherst, shreyas.panse@gmail.com

BACKGROUND AND AVAILABLE POTENTIAL ENERGY IN NUMERICAL SIMULATIONS OF A BOUSSINESQ FLUID

A Thesis Presented

by

SHREYAS S. PANSE

Submitted to the Graduate School of the
University of Massachusetts Amherst in partial fulfillment
of the requirements for the degree of

MASTER OF SCIENCE IN MECHANICAL ENGINEERING

February 2013

Mechanical and Industrial Engineering

BACKGROUND AND AVAILABLE POTENTIAL ENERGY IN NUMERICAL SIMULATIONS OF A BOUSSINESQ FLUID

A Thesis Presented

by

SHREYAS S. PANSE

Approved as to style and content by:

Stephen de Bruyn Kops, Chair

David Schmidt, Member

Yahya Modarres-Sadeghi, Member

Donald Fisher, Department Head
Mechanical and Industrial Engineering

To my mother and father

ACKNOWLEDGMENTS

I would like to gratefully acknowledge the generous funding provided from the Office of Naval Research, Grant Number N00014-08-1-0236.

I would like to thank Prof. Stephen de Bruyn Kops for his guidance and support throughout the course of this research.

Thanks to Prof. David Schmidt for useful comments and discussions on the stochastic methods.

ABSTRACT

BACKGROUND AND AVAILABLE POTENTIAL ENERGY IN NUMERICAL SIMULATIONS OF A BOUSSINESQ FLUID

FEBRUARY 2013

SHREYAS S. PANSE

M.S.M.E., UNIVERSITY OF MASSACHUSETTS AMHERST

Directed by: Professor Stephen de Bruyn Kops

In flows with stable density stratification, a portion of the gravitational potential energy is available for conversion to kinetic energy. The remainder is not and is called "background potential energy". The partition of potential energy is analogous to the classical division of energy due to motion into its kinetic and internal components. Computing background and available potential energies is important for understanding stratified flows. In many numerical simulations, though, the Boussinesq approximations to the Navier-Stokes equations are employed. These approximations are not consistent with conservation of energy. In this thesis we re-derive the governing equations for a buoyancy driven fluid using Boussinesq approximations. Analytical and stochastic approaches to partitioning potential energy are developed and analyzed in simplified 1-D cases. Finally, ambient and deviatoric potential energies, quantities analogous to background and available potential energy are introduced. Direct Numerical Simulations are used to formulate an energy budget. The actual and surrogate potential energies are compared based on the simulation results.

TABLE OF CONTENTS

LIST OF TABLES

Table **Page**

LIST OF FIGURES

Figure **Page**

CHAPTER 1

INTRODUCTION AND BACKGROUND

In the simulation and modeling of fluid flows affected by buoyancy, the assumptions of Boussinesq [1903] are very often used to simplify the equations of motion. Spiegel and Veronis [1960] introduced the now common approach of showing under what conditions the errors in the Boussinesq approximation are small. For instance, the velocity in the atmosphere over a limited vertical range can be expected to be very nearly non-divergent. In numerical simulations, however, the Boussinesq approximations are taken literally. Typically the evolution equations for momentum and temperature are solved numerically with the constraint that the velocity be non-divergent. The result is that neither mass nor energy is conserved locally. We use the term "Boussinesq fluid" to describe the simulated fluid which, unlike a real fluid being approximated by the Boussinesq assumptions, does not obey the laws of physics, at least locally. In particular we consider the implications of studying potential energy dynamics using direct numerical simulations (DNSs) since the value of these simulations is generally accepted to stem from their high resolution in space and time.

In flows strongly influenced by gravity, a significant amount of energy may be in the form of potential energy. Lorenz [1955] recognized that much of this energy is not actually available to do work and introduced the concepts of available and reference, or background, potential energies. The rate at which available potential energy is lost to background potential energy via molecular mixing is analogous to the so-called dissipation rate of kinetic energy, or the irreversible conversion of kinetic to internal energy. So understanding the dynamics of potential energy is central to

understanding geophysical flows and the topic has been the subject of numerous numerical simulations. Unfortunately, accurately computing available and background potential energies in an arbitrary control volume is a numerical challenge made more challenging by the fact that solutions to the Boussinesq equations are not energy conserving.

In short, this study addresses two challenging topics in simulations of buoyancy driven flows, 1) the Boussinesq approximations and 2) the accurate partitioning of potential energy at a local level in numerical simulations. Even though both of these topics play a significant role in variety of applications, the examples used in this study are more common to atmospheric and oceanic research.

To better acquaint the reader with the basic concepts, potential energy dynamics and Boussinesq approximations are briefly reviewed along with the relevant literature, in §1.1. In the following section (§1.2) the governing equations for a fluid following the Boussinesq approximations are rigorously derived to reveal the "laws" obeyed by a Boussinesq fluid, in particular in the context of local energy balances. In chapter 2, the concepts of partitioning potential energy into available and background components using a stochastic approach are presented in a way that facilitates computing their local values exactly for certain analytical problems (chapter 3) and very accurately in numerical simulations(chapter 4). In the course of this research, we have come to the conclusion that the numerical error in the local values of available potential energy is the result of vertical descritization. When the stochastic approach is applied to multifarious 2-D and 3-D problems the descritization errors are compounded further. As a workaround to this problem, we introduce ambient and deviatoric potential energies, quantities analogous background and available potential energies in chapter 5. In doing so, we follow the definition of available potential energy by Holliday and McIntyre [1981]. Finally, the available and background potential energies are com-

pared with its surrogate quantities using the results of direct numerical simulations in chapter 6 and conclusions are discussed in chapters 7.

1.1 Literature Review

In stratified fluids, buoyancy effects due to gravity interacting with density gradient leads to either horizontal stratification or vertical convection. Effects of variable density are crucial in understanding stratified flows and the best place to start are the fully compressible Navier Stokes equations. The equations for conservation of mass, momentum, energy for fully compressible flow of a Newtonian fluid are listed below.

$$\left[\frac{\partial \rho}{\partial t} + \boldsymbol{v} \cdot \nabla \rho\right] = -\rho \nabla \cdot \boldsymbol{v}, \tag{1.1a}$$

$$\rho \left[\frac{\partial \boldsymbol{v}}{\partial t} + \boldsymbol{v} \cdot \nabla \boldsymbol{v}\right] = -\nabla p + \rho g - \frac{2}{3}\nabla(\mu \nabla \cdot \boldsymbol{v}) + 2\nabla \cdot (\mu \mathbf{S}), \tag{1.1b}$$

$$\rho c_p \left[\frac{\partial T}{\partial t} + \boldsymbol{v} \cdot \nabla T\right] = \nabla \cdot (\kappa \nabla T) - \frac{2}{3}\mu(\nabla \cdot \boldsymbol{v})^2 + 2\mu \mathbf{S} \colon \mathbf{S} + \beta T \frac{Dp}{Dt}, \tag{1.1c}$$

where $\mathbf{S}$ is the strain rate tensor [Panton, 1996].

The fully compressible governing equations written above allow acoustic modes in a simulation. The energy associated with the acoustic waves is very small as compared to the kinetic energy and internal energy can be safely ignored, in case of low Mach number. However, their presence has a severe limitation on the maximum size of a time step in numerical simulations, if an explicit time-stepping is used. In DNSs, all dynamically relevant length and time scales are resolved. To resolve acoustic waves in time requires a time step much smaller than any time scale relevant to the turbulence. This motivates removing the waves from the governing equations. The

maximum permissible time step has to follow the Courant-Friedrichs-Lewy (CFL) condition [Xu et al., 1992],

$$\Delta t \leq \Delta s / C_s,$$

where Δs is the spatial increment and C_s is the speed of fastest acoustic wave. In order to use larger time steps it is necessary to filter out acoustic waves from the simulation.

Various approximations are applied to the governing equations to eliminate acoustic waves from the simulations. Different approaches to studying variable density flows can be employed depending on the context. In aerodynamics, the fluctuation in density can be attributed to compressibility effects due to high Mach number. Zero Mach number approach is used while dealing with engineering flows with density variations due to heating or mixing. In geophysical fluid dynamics, the density variation is treated under the confines of the Boussinesq approximation. In many cases, changes in density are considered negligible and thus ignored. This leads to the incompressible assumption. A few of these notable assumptions are addressed in the following sections.

1.1.1 Limiting Cases Derived Analytically

1.1.1.1 Zero Mach Number Approach

The fundamental idea behind the zero Mach number approach is that the velocity (and frequency) of acoustic waves (resulting from perturbations in flow or exothermic processes such as combustion or chemical reactions) is very high as compared to the velocity of convection of the flow. It follows from the asymptotic limit (Mach number goes to zero) that the speed of sound will become infinity, for a non zero flow velocity.

$$M \to 0, c \to \infty \quad where\ M = \frac{U}{c}.$$

Hence the changes in thermodynamic pressure are realized instantaneously throughout the flow. In other words, zero Mach number ensures uniform thermodynamic pressure distribution, i.e., $\nabla\, p_t = 0$, and consequently isolates density changes due to fluctuations in temperature.

Fundamental mathematics of zero Mach number approach in compressible and incompressible flows can be found in Klainerman and Majda [1982]. More applications of the zero Mach number approach in numerical simulations can be found in Klainerman and Majda [1982] and Cook and Riley [1996]. McMurtry et al. [1986] derived approximate equations for zero Mach number flow and validated by comparing the results from full compressible governing equations (1.1) in a simulation of reacting mixing layer with chemical heat release. Jang and de Bruyn Kops [2007] also use zero Mach number approach in Direct Numerical Simulations (DNSs) of turbulent mixing layers with high density ratios.

1.1.1.2 Incompressible Assumption

Incompressible flow is a term that is applied to any situation where the changes in density for a fluid parcel are assumed to be negligible. From continuity equation it follows that

$$\frac{1}{\rho}\frac{D\rho}{Dt} = 0 \quad \text{or} \quad \nabla \cdot \boldsymbol{u} = 0.$$

Fluid parcels are allowed to have different densities from each other, however the density of each parcel should remain unchanged. The basic requirement for a flow to be incompressible is that the Mach number should be restricted to low values ($M \rightarrow 0$). That means all velocities in a fluid must be small as compared to the speed of sound. Considering density fluctuations as a result of changes in pressure at any particular location in the flow, it follows that

$$M^2 = \frac{\nabla\rho}{\rho_m},$$

where ρ_m is the mean density of the flow [Panton, 1996]. Therefore M^2 is an indicator of density fluctuations with respect to the mean fluid density. As $M^2 \to 0$, the density changes are only a small fraction of density of a fluid parcel.

An important aspect of the incompressible assumption is that the momentum and continuity equations are decoupled from the energy equation. It is possible to solve for the three velocities (u, v and w) and pressure without considering the energy equation (temperature). In other words, the velocity field in incompressible flow is independent of heat transfer or thermal effects and hence non-divergent.

There is a great deal of material covering mathematical derivation and applications on incompressible flows. Panton [1996] cover the fundamentals of incompressible flows in more detail.

1.1.2 Order of Magnitude Estimations

1.1.2.1 Boundary Layer Approximation

At high Reynolds numbers, the viscous effects in a flow are assumed to be negligible and the fluid is assumed to be inviscid. The problem with the inviscid model is that it cannot satisfy the no-slip boundary condition (i.e. the condition that restricts fluid velocity at a solid surface to zero). No-slip boundary conditions result in steep velocity gradients normal to the solid surface in contact with the fluid. The inviscid model, in any case, cannot account for these velocity gradients in the fluid. It was Prandtl in 1904, who suggested a specialized region very near the surface known as the *boundary layer*, wherein the viscous effects are significant irrespective of the Reynolds number. Thickness of the boundary layer, however, decreases with higher Reynolds numbers.

The reason inviscid-flow theory fails to account for no-slip boundary conditions is that the viscous effects do not occur at the characteristic length scale of the flow (L). The natural scale in the direction normal to the surface is δ, the thickness of the

boundary layer. It is important to note that,

$$Re \to \infty, \delta \to 0.$$

When the three momentum equations are scaled by L and δ, only the longitudinal convection term and one of the viscous terms are retained and this provides enough flexibility to account for no-slip boundary conditions. Panton [1996] and Bird et al. [2002] discuss the boundary layer approximation and the governing equations in two and three dimensions in great detail.

The boundary layer approximation is pertinent to our discussion because it follows a similar order of magnitude analysis as is used in deriving the Boussinesq approximation.

1.1.2.2 Boussinesq Approximation

While dealing with compressible flows in density stratified fluids, the Boussinesq approximation is the most commonly used to simplify the equations governing the flow. Boussinesq [1903] introduced the approximation that the difference in density within a fluid or between two mixing fluids is negligible, except when the density term is multiplied by gravity. (This approximation is similar to the boundary layer in which viscosity is important only in certain areas of the flow). Spiegel and Veronis [1960] identified the conditions under which Boussinesq approximation is valid.

We can write an equation of state of a general fluid as

$$\frac{1}{\rho}\frac{D\rho}{Dt} = \beta\frac{Dp}{Dt} - \alpha\frac{DT}{Dt},$$

where β is the isothermal compressibility and α is the thermal expansion coefficient. Thermodynamic variables α and β characterize a fluid. By assuming restrictions on either or both, compressible governing equations can be simplified to solve various types of flows.

In the Boussinesq approximation, it is assumed that the changes in density due to motion of the fluid are primarily due to thermal effects as opposed to pressure effects. This leads to the assumption that the thermal expansion coefficient (α) is much greater than the isothermal compressibility (β), which is considered negligible:

$$\alpha \gg \beta.$$

Temperature differences alone cause changes in density as in thermal convection. This assumption is diametrically opposite to the one made in confined flows where thermal expansion coefficient (α) is considered negligible, as compared to β.

Similar to the boundary layer approximation, where the viscosity of the fluid is taken into account only at the boundaries, the Boussinesq approximation considers density fluctuation only when it is coupled with gravity. It is useful to express the state variables such as pressure, density and temperature as a sum of mean and fluctuating parts. Assume that ψ is a state variable then,

$$\psi(\boldsymbol{x}, t) = \psi_m + \overline{\psi}(z) + \psi'(\boldsymbol{x}, t),$$

where ψ_m is the mean of ψ, $\overline{\psi}$ is the horizontal variation in ψ in the absence of motion and ψ' is the dynamic (temporal) fluctuation resulting from motion. The Boussinesq approximation assumes that the dynamic perturbations in density ρ' are small as compared to the background mean density (ρ_m). This assumption allows us to linearize any term involving product with density (eg. $\rho \overrightarrow{\boldsymbol{v}} \rightarrow \rho_m \overrightarrow{\boldsymbol{v}}$).

The Boussinesq approximation is classified into hydrostatic and non-hydrostatic (anelastic) Boussinesq approximation. The Hydrostatic Boussinesq assumption states that the acceleration of vertical velocity is small as compared to the other terms in the vertical component of momentum equation, ($\frac{\partial \boldsymbol{w}}{\partial t} = 0$). The equation reduces to,

$$\frac{\partial p}{\partial z} = -\rho g.$$

As mentioned earlier, the Boussinesq approximation requires,

$$\rho_m \gg \overline{\rho} \gg \rho'. \tag{1.2}$$

From (1.2) and the fact that ρ_m is constant, continuity equation reduces to an incompressible form,

$$\nabla \cdot u = 0.$$

Thus, hydrostatic Boussinesq assumption ensures conservation of volume at the expense of conservation of mass. This is a good approximation for the ocean where, the (1.2) is fulfilled.

Equation (1.2) is a good approximation for the ocean as liquids are incompressible, but not so good for the troposphere (first 15 km of the atmosphere). In the later case, $\overline{\rho}$ and ρ_m are very large and in such a case the non-hydrostatic (anelastic) Boussinesq approximation is used. The anelastic approximation assumes that,

$$\rho = \overline{\rho}(z) + \rho'(\boldsymbol{x}, t) \text{ and } \quad \overline{\rho} \gg \rho'.$$

Hence the continuity equation now becomes,

$$\nabla \cdot (\overline{\rho}\boldsymbol{u}) = 0.$$

This is a pseudo-incompressible form of the continuity equation for which assumptions and the derivation are included in Ogura and Phillips [1961]. In the anelastic approximation, volume is not conserved but mass in conserved in the vertical direction.

Both hydrostatic and non-hydrostatic models are effective in modeling shallow convection. But for deep convection, the effect of changes in dynamic pressure on

temperature may be significant enough so as not to be ignored, as is customary in the Boussinesq approximations. Mihaljan [1962] follow a series expansion approach rather than a order of magnitude approach to derive governing equations for a Boussinesq fluid. Instead of following (1.2), small terms in state variables (density and pressure) are eliminated based on series expansion. Spiegel and Veronis [1960] on the other hand, introduce a scale height such that,

$$D_f = \mid \frac{1}{\psi_m}\frac{d\overline{\psi}}{dz} \mid^{-1},$$

and any layer under consideration should have a thickness (d) very less than the scale height ($d << D_f$). It follows from this requirement that $\Delta\overline{\rho}/\rho_m << 1$. This is the basic condition that must be satisfied for any convection problem. Spiegel and Veronis [1960] derive the governing equations for Boussinesq approximation based on above restrictions and are listed below for reference.

$$\nabla \cdot \boldsymbol{v} = 0, \tag{1.3a}$$

$$\frac{\partial \boldsymbol{v}}{\partial t} + \boldsymbol{v} \cdot \nabla \boldsymbol{v} = -\frac{1}{\rho_m}\nabla p' + g\alpha T'\boldsymbol{k} + \nu\nabla^2 \boldsymbol{v}, \tag{1.3b}$$

$$\frac{\rho'}{\rho_m} = \frac{T'}{T_m} = -\alpha_m T', \tag{1.3c}$$

$$\frac{DT'}{Dt} + \boldsymbol{w}\left(\frac{\partial T_0}{\partial z} + \frac{g}{C_p}\right) = K\nabla^2 T' + \frac{Q'}{\rho_m C_p}, \tag{1.3d}$$

where Q' is heat transfer by radiation, which is not included in this study [Spiegel and Veronis, 1960]. Governing equations for a Boussinesq fluid in this study are derived by following the series expansion in Mihaljan [1962] and are listed as (1.10), (1.10b) and (1.10c) in §1.2

1.1.3 Available Potential Energy and Energy Budget

Lorenz [1955] introduced the concept of available potential energy while discussing the maintenance of general circulation in the atmosphere and defined the conservation

of available potential energy and kinetic energy. Holliday and McIntyre [1981] derived exact equations for potential energy and formulated a budget of kinetic and potential energy in stratified inviscid incompressible flows. Mihaljan [1962] rigorously derived governing equations for a Boussinesq fluid as well as equations for kinetic, potential and internal energies, applied these equations to solve a thermal convection problem and discussed energetics based on the system of derived equations. Winters et al. [1995] derived volumetric evolution equations for background and available potential energy for a Boussinesq fluid and applied them to mixing problems in stratified fluids to formulate an energy budget.

Lorenz [1955] defines available potential energy as the part of total potential energy that is available for conversion with kinetic energy. Available potential energy is defined as the difference between the total potential energy in a stratified fluid at any given point of time and the total potential energy of the fluid if it were redistributed to its most stable state. It is defined for a fixed volume containing a fixed mass as in the atmosphere. In Lorenz [1955], the author discusses critical modes of conversion of available potential energy in the context of large scales of general circulation.

Diffusive mixing is one way of energy transfer which acts towards smoothing density gradients and thus altering the potential energy of the fluid. Winters et al. [1995] provide an insight into energetics of mixing in a Boussinesq fluid, primarily focusing on density stratified turbulence characterized by dissipation and diapycnal mixing.

Tseng and Ferziger [2001] explain the difference between mixing and stirring processes in the context of stratified flows. Stirring is a mechanical process through which fluid elements of different densities are bought in contact and kinetic energy in converted into potential energy. While mixing is a process of diffusion across interfaces of different densities (diapycnal surfaces) and is irreversible under the influence of gravity.

Mixing is parameterized by the following dimensionless groups:

Prandtl Number (Pr): It is the ratio of viscous diffusion rate to thermal diffusion rate. Under Boussinesq approximation, the thermal diffusion rate is of primary importance.

Schmidt Number (Sc): It is the ratio of viscous diffusion rate to mass (molecular) diffusion rate. Boussinesq equation of state for an ideal gas links thermal diffusion to molecular diffusion.

Froude Number (Fr): It is the ratio of characteristic velocity of the fluid to the wave propagation velocity. Froude number is analogous to the Mach number.

The approach of Mihaljan [1962] is based on Rayleigh number, Peclet number and two other non-dimensional parameters (ϵ_1 and ϵ_2). These are defined in terms of isothermal compressibility (β), which is considered negligible. Series expansion of dependant variables (p, ρ and θ) in terms of these two parameters and exclusion of higher order terms in the governing equations leads evolution equation for energy in a Boussinesq fluid. The details of this approach are discussed in detail in §1.2.1.

Winters et al. [1995] derive and apply volumetric equations for background and available potential energies and apply the equations in 2D and 3D simulations of mixing in a stratified fluid and formulated an energy budget for a fixed volume of fluid. One of the key features of their energy budget is the ability to differentiate the changes in potential energy as diabatic and adiabatic. They complete the energy budget by computing the fluxes and conversion rates of energy. Winters et al. [1995] provide an ideal framework for study of energetics in Boussinesq fluid.

1.1.4 Numerical Implementation

Partitioning potential energy into background and available potential energy depends on our ability to find a reference state of the fluid $\rho(z_*)$ (adiabatically redistributed to the lowest energy state). Finding the reference state mathematically is

relatively straightforward (see chapter 2), but numerically computing an exact reference state for a given density field is a challenge.

Winters et al. [1995] follow Thorpe's reordering approach. Essentially they sort a three dimensional field of discrete fluid elements into one dimensional array of sorted elements, which are then distributed in the original grid to get an approximation of an adiabatically redistributed fluid. However this approach is only suitable for horizontally homogeneous field. This is because in an approximated field, a single horizontal layer of fluid elements consists of elements with different densities. This is different from a real fluid where an isopycnal layer will adjust itself to remain perpendicular to the vertical density gradient. Irrespective of our ability to sort a density field, accuracy of Thorpe's reordering approach depends on the number of sampled locations [Tseng and Ferziger, 2001].

Tseng and Ferziger [2001] summarize various approaches of computing the reference states and introduce a stochastic approach based on computing the probability density function (PDF) of the density. They apply this approach to a lid-driven cavity flow to complete an energy budget by following energy equations from Winters et al. [1995].

The stochastic approach presented by Tseng and Ferziger [2001] is exactly the same as sorting yet it manages to maintain horizontal homogeneity and therefore presents a very accurate model of a reference state. To improve accuracy they apply an adaptive mesh in computing the PDF of any given field. Instead of discretizing the given field in an uniform grid, they use Chebyshev transformations to discretize whenever the program detects steep density gradients (near the upper and lower bounds of probability space).

The pdf method discussed by Tseng and Ferziger [2001] is the one of the fundamental approaches followed in the numerical implementation in this thesis. In the 3-D implementation of this stochastic approach, however, the available potential energy is

prone to significant discretization errors. Therefore, ambient and deviatoric potential energies, analogous to background and available potential energies, are introduced, developed in chapter 5 and the corresponding energy budget is compared in chapter 6.

1.2 Background

1.2.1 Continuity, Momentum, and Temperature

Fundamental to the Boussinesq approximation is the constraint that the isothermal compressibility of the fluid, $\hat{\beta}$, be negligible compared with the thermal expansion coefficient, $\hat{\alpha}$, which leads to the equation of state

$$\hat{\rho} = \hat{\rho_0}(1 - \hat{\alpha}\hat{\theta}), \tag{1.4}$$

where $\hat{\rho}$ is the fluid density, $\hat{\rho_0}$ is the density at the reference temperature $\hat{T}_0$, and $\hat{\theta} = \hat{T} - \hat{T}_0$ is the departure of the temperature, $\hat{T}$, from the reference state. The notation $\hat{(\,)}$ indicates a dimensional quantity. Given this equation of state, the remaining assumptions in the Boussinesq approximation follow Spiegel and Veronis [1960] and Mihaljan [1962]. For our purpose, the rigorous approach of Mihaljan [1962] is informative and so we use it for guidance in the foregoing analysis of the energetics of a Boussinesq fluid, that is, the energetics described by numerical solutions to the Boussinesq equations

The dimensional problem statement involves 11 dimensional parameters (6 thermophysical properties of the fluid, the gravitational constant, and 4 scaling parameters):

$\hat{C}_p$, Specific heat at constant pressure

$\hat{C}_v$, Specific heat at constant volume

$\hat{\mu}$, Molecular viscosity

$\hat{\lambda}$, Dilatation viscosity

$\hat{k}$, Thermal conductivity

$\hat{\alpha}$, Thermal expansion coefficient

$\hat{g}$, Gravitational acceleration

$\hat{\rho}_0$, Reference density

$\hat{V}$, Characteristic velocity scale

$\hat{L}$, Characteristic length scale

$\hat{\Theta}$, Characteristic temperature scale.

There are four dimensions (mass, length, time, and temperature). Thus, from Buckingham's Pi theorem we expect seven dimensionless groups. Scaling pressure by $\hat{\rho}_0\hat{V}^2$ and time by $\hat{L}/\hat{V}$, we choose these groups to be:

$$\pi_1 = \hat{\alpha}\hat{\Theta} \qquad \pi_2 = \frac{\hat{V}^2}{\hat{C}_p\hat{\Theta}} \tag{1.5}$$

$$\mathrm{Re} = \frac{\hat{\rho}_0\hat{V}\hat{L}}{\hat{\mu}} \qquad \mathrm{F}^2 = \frac{\hat{V}^2}{\hat{\alpha}\hat{\Theta}\hat{g}\hat{L}} \tag{1.6}$$

$$\mathrm{Pr} = \frac{\hat{C}_p\hat{\mu}}{\hat{k}} \qquad \gamma = \frac{\hat{C}_p}{\hat{C}_v} \tag{1.7}$$

$$\lambda = \frac{\hat{\lambda}}{\hat{\mu}}\ . \tag{1.8}$$

The definition of F^2 may be unexpected and will be discussed once the derivation of the Boussinesq equations has been completed.

Non-dimensionalized as above and incorporating the equation of state 1.4, the equations for continuity, momentum, and temperature are

$$-\pi_1\frac{D\theta}{Dt} = -(1-\pi_1\theta)\,(\nabla\cdot\boldsymbol{v}) \tag{1.9a}$$

$$(1-\pi_1\theta)\frac{D\boldsymbol{v}}{Dt} = -\nabla p - \frac{1}{\mathrm{Re}}\left[\nabla\cdot\boldsymbol{\tau}\right] + \frac{1}{\mathrm{F}^2}\theta\boldsymbol{\delta}_z \tag{1.9b}$$

$$(1-\pi_1\theta)\frac{D\theta}{Dt} = \frac{1}{\mathrm{Pr\ Re}}\nabla^2\theta - \pi_2\left[\frac{1}{\mathrm{Re}}\left(\boldsymbol{\tau}:\nabla\boldsymbol{v}\right) + \frac{\pi_1 T}{1-\pi_1}\left(\frac{Dp}{Dt} - \frac{1}{\pi_1\mathrm{F}^2}w\right)\right] \tag{1.9c}$$

with

$$\boldsymbol{\tau} = -(\nabla\boldsymbol{v} + (\nabla\boldsymbol{v})^T) + \left(\frac{2}{3} - \lambda\right)(\nabla\cdot\boldsymbol{v})\,\boldsymbol{\delta}$$

and

$$\nabla\cdot\boldsymbol{q} = -k\nabla^2 T\ .$$

The superscript $(\ )^T$ indicates the transpose of the tensor and $\boldsymbol{\delta}$ is the unit tensor. The velocity vector is $\boldsymbol{v} = \{u, v, w\}$, p is the sum of the thermodynamic and hydrostatic pressures,

$$p = p_t + \frac{1}{\pi_1}\frac{1}{\mathrm{F}^2}z$$

and $\rho\boldsymbol{\delta}_z g$ is the body force vector of magnitude g in the negative z-direction so that $\nabla\Phi_\rho = \boldsymbol{\delta}_z \mathrm{g}$ with $\boldsymbol{\delta}_z$ the unit vector in the z-direction and the subscript 'ρ' indicates energy per unit mass.

The choice of definition for F^2 becomes apparent when $\boldsymbol{v}$, θ, and p in (1.9) are replaced by power series expansions in terms of π_1 and π_2. Using the notation of Mihaljan [1962], let ξ be any one of the variables $\boldsymbol{v}$, p, and θ and write $\xi = \xi^{0,0} + \pi_1\xi^{1,0} + \pi_2\xi^{0,1} + \pi_1\pi_2\xi^{1,1} + ...$ Retaining only the zeroth order terms results in the Boussinesq equations for continuity, momentum, and temperature:

$$\nabla\cdot\boldsymbol{v}^{0,0} = 0 \tag{1.10a}$$

$$\frac{D\boldsymbol{v}^{0,0}}{Dt} = -\nabla p^{0,0} - \frac{1}{\mathrm{Re}}\left[\nabla\cdot\boldsymbol{\tau}^{0,0}\right] + \frac{1}{\mathrm{F}^2}\theta^{0,0}\boldsymbol{\delta}_z \tag{1.10b}$$

$$\frac{D\theta^{0,0}}{Dt} = \frac{1}{\mathrm{Pr\ Re}}\nabla^2\theta^{0,0} \tag{1.10c}$$

with

$$\boldsymbol{\tau}^{0,0} = -(\nabla\boldsymbol{v}^{0,0} + (\nabla\boldsymbol{v}^{0,0})^T)\ .$$

If F^2 were defined without $\hat{\alpha}\hat{\Theta}$ in the denominator then the series expansion step would result in the equations for an incompressible flow with θ as a passive scalar. We consider F^2 to be a Froude number but it might also be taken as the Reynolds number squared divided by the Grashof number. Also, π_2 is sometimes referred to as the Brinkman number divided by the Prandtl number (c.f. [Bird et al., 2002]).

1.2.2 Exact Energy Equations with zero Isothermmal Compressibility (β)

Equations (1.10) describe the flow of a Boussinesq fluid and we previously referred to them as the "the Boussinesq equations." Deriving them by non-dimensionalizing the full equations and expanding them in terms of π_1 and π_2 is rigorous and easily applied to the transport equations for kinetic, internal, and potential energies to understand the energetics of a Boussinesq fluid. The dimensional kinetic, internal, and potential energies per unit volume are defined within the Boussinesq approximation as $\hat{K} = \hat{\rho}_0\hat{V}^2/2$, $\hat{U} = \hat{\rho}_0\hat{C}_v\hat{\theta}$, and $\hat{\Phi} = (1 - \hat{\alpha}\hat{\theta})\hat{g}\hat{z}$, respectively. Since high Reynolds number flows motivate this discussion, it is natural to non-dimensionalize energy by $\hat{\rho}_0\hat{V}^2$ whereby $K = \hat{K}/\hat{\rho}_0\hat{V}^2$, $U = \hat{U}/\hat{\rho}_0\hat{C}_v\hat{\Theta}\pi_2\gamma$, and $\Phi = \hat{\Phi}/\hat{\rho}_0\hat{g}\hat{L}\pi_1\mathrm{F}^2$. The dimensionless energy equations are:

$$\frac{DK}{Dt} = -(\boldsymbol{v}\cdot\nabla p) - \frac{\boldsymbol{v}\cdot[\nabla\cdot\boldsymbol{\tau}])}{\mathrm{Re}} + \frac{\theta w}{\mathrm{F}^2} \tag{1.11a}$$

$$\frac{DU}{Dt} = \frac{\nabla^2\theta}{\mathrm{Pr}\ \mathrm{Re}\ \pi_2} - p(\nabla\cdot\boldsymbol{v}) - \frac{\boldsymbol{\tau}:\nabla\boldsymbol{v}}{\mathrm{Re}} + \frac{z\nabla\cdot\boldsymbol{v}}{\pi_1\ \mathrm{F}^2} \tag{1.11b}$$

$$\frac{D\Phi}{Dt} = -\frac{z\nabla^2\theta}{\mathrm{Pr}\ \mathrm{Re}\ \mathrm{F}^2} + \frac{w}{\pi_1\ \mathrm{F}^2} - \frac{\theta w}{\mathrm{F}^2} \tag{1.11c}$$

$$\frac{D}{Dt}\left[K + U + \Phi\right] = \left[\frac{1}{\pi_2} - \frac{z}{\mathrm{F}^2}\right]\frac{\nabla^2\theta}{\mathrm{Pr}\ \mathrm{Re}} - (\nabla\cdot p\boldsymbol{v}) - \frac{\nabla\cdot[\boldsymbol{\tau}\cdot\boldsymbol{v}]}{\mathrm{Re}} + \frac{\nabla\cdot(z\boldsymbol{v})}{\pi_1\ \mathrm{F}^2} \tag{1.11d}$$

The first term in the (1.11c) can be written as $-\nabla\cdot[z\nabla\theta - \theta\nabla z]$ and this when integrated over the volume gives us change in energy due to *diffusive flux* of heat or mass and Boussinesq form of conversion rate from internal to potential energy (ϕ_i) [Winters et al., 1995]. It is common to integrate (1.11) over a control volume

(c.f. [Mihaljan, 1962, Winters et al., 1995]) to simplify the identification of the various terms with physical processes. We do not do this as our interest is in the local quantities. Now let us derive the Boussinesq energy equations. This is done formally by expanding (1.11) in power series in terms of π_1 and π_2 and retaining the lowest order terms:

$$\frac{DK^{0,0}}{Dt} = -\left(\boldsymbol{v}^{0,0}\cdot\nabla p^{0,0}\right) - \frac{(\boldsymbol{v}^{0,0}\cdot[\nabla\cdot\boldsymbol{\tau}^{0,0}])}{\mathrm{Re}} + \frac{\theta^{0,0}w^{0,0}}{\mathrm{F}^2} \quad (1.12a)$$

$$\frac{DU^{0,0}}{Dt} = \frac{\nabla^2(\theta^{0,0}+\pi_1\theta^{1,0}+\pi_2\theta^{0,1})}{\pi_2\ \mathrm{Pr}\ \mathrm{Re}} - \frac{\boldsymbol{\tau}^{0,0}:\nabla\boldsymbol{v}^{0,0}}{\mathrm{Re}} + \frac{z\nabla\cdot\boldsymbol{v}^{1,0}}{\mathrm{F}^2} \quad (1.12b)$$

$$\frac{D\Phi^{0,0}}{Dt} = -\frac{z^{0,0}\nabla^2(\theta^{0,0}+\pi_1\theta^{1,0})}{\mathrm{Pr}\ \mathrm{Re}\ \mathrm{F}^2} + \frac{w^{0,0}+\pi_1 w^{1,0}}{\pi_1\ \mathrm{F}^2} - \frac{\theta^{0,0}w^{0,0}}{\mathrm{F}^2}\ , \quad (1.12c)$$

where

$$K^{0,0} = \boldsymbol{v}^{0,0}\cdot\boldsymbol{v}^{0,0}$$
$$U^{0,0} = \frac{1}{\pi_2\gamma}(\theta^{0,0}+\pi_1(\theta^{0,0})^2+\pi_1\theta^{1,0}+\pi_2\theta^{0,1})$$
$$\Phi^{0,0} = \frac{1}{\pi_1\mathrm{F}^2}(1+\pi_1\theta^{0,0})\ z$$

1.2.3 Implied Energy Equations for Boussinesq fluid

Equations (1.12) are formally derived using the same approach used to derive the Boussinesq equations (1.10). The implications of the energy equations are discussed in chapter 3, but a cursory review of (1.12) reveals that they involve quantities that are not available in simulations based on the solution of (1.10), e.g., $\theta^{1,0}$. Using just quantities computed directly from (1.10), approximate energy equations can be obtained. The equation for kinetic energy results from the dot product of velocity with (1.10b) and the equation for internal energy is (1.10c) divided by π_2. The

potential energy equation follows from the kinetic energy equation and the definition of potential energy. Therefore, the energy equations based on (1.10) are

$$\frac{DK_\rho^{0,0}}{Dt} = -\left(\boldsymbol{v}^{0,0}\cdot\nabla p^{0,0}\right) - \frac{(\boldsymbol{v}^{0,0}\cdot[\nabla\cdot\boldsymbol{\tau}^{0,0}])}{\mathrm{Re}} + \frac{\theta^{0,0}w^{0,0}}{\mathrm{F}^2} \tag{1.13a}$$

$$\frac{DU_\rho^{0,0}}{Dt} = \frac{\nabla^2\theta^{0,0}}{\pi_2\ \mathrm{Pr}\ \mathrm{Re}} \tag{1.13b}$$

$$\frac{D\Phi_\rho^{0,0}}{Dt} = -\frac{z\nabla^2\theta^{0,0}}{\mathrm{Pr}\ \mathrm{Re}\ \mathrm{F}^2} - \frac{\theta^{0,0}w^{0,0}}{\mathrm{F}^2}\ . \tag{1.13c}$$

CHAPTER 2

THEORETICAL CONCEPTS FOR PARTITIONING POTENTIAL ENERGY

2.1 Available and Background Potential Energy

When a flow is allowed to settle reversibly to its lowest potential energy state, the resulting potential energy is the "background potential energy", Φ_b [Lorenz, 1955]. The background potential energy is unavailable for exchange with kinetic energy via the buoyancy flux, $\theta w/\mathrm{F}^2$. The "available potential energy" is the difference between the total and background potential energies: $\Phi_a = \Phi - \Phi_b$. Holliday and McIntyre [1981] and Winters et al. [1995] provide two approaches to deriving a dynamic equation for Φ_a. The former assumes an inviscid fluid while the latter focuses on the integral of Φ_a over a control volume. Our interest is the local quantity for a real fluid. Paradoxically, Φ, Φ_a, and Φ_b are local quantities but Φ_a and Φ_b can only be determined in the context of a volume of fluid since the fraction of Φ in a fluid element that can be reversibly converted to kinetic energy depends on the state of all the other fluid elements in the volume.

Several methods for determining Φ_b that are reviewed by Tseng and Ferziger [2001]. Perhaps the most intuitive with regards to Lorenz's definition of background potential energy is to sort the density field and define the resulting elevation of a fluid element above a reference level as $Z_*(\boldsymbol{x}, t)$. Then the background and available potential energy per unit volume are

$$\Phi_b = \frac{\rho}{\pi_1 \mathrm{F}^2} Z_* \ , \qquad \Phi_a = \frac{\rho}{\pi_1 \mathrm{F}^2}(z - Z_*) \ .$$

Tseng and Ferziger [2001] show that Φ_b can be expressed in terms of the probability density function (PDF) of ρ , $f(\tilde{\rho};\boldsymbol{x},t)$. with $\tilde{\rho}$ being the sample-space analog of ρ. We arrive at the same result but begin by letting the PDF of ρ as a function of space and time,

$$f^*_\rho(\tilde{\rho};\boldsymbol{x},t) \equiv \delta(\rho(\boldsymbol{x},t) - \tilde{\rho}) \ , \tag{2.1}$$

be a random variable. [Pope, 2000] refers to f^*_ρ as the "fine-grained" PDF. Denoting the expected value of a random variable by $\langle\ \rangle_e$,

$$f_\rho(\tilde{\rho};\boldsymbol{x},t) = \left\langle f^*_\rho(\tilde{\rho};\boldsymbol{x},t)\right\rangle_e \ . \tag{2.2}$$

This is simply a property of a random variable and is inherent in the definition of a fine-grained PDF. The distribution function, $F_\rho(\tilde{\rho};\boldsymbol{x},t)$, gives the probability that $\rho \leq \tilde{\rho}$. The relationship between F_ρ and f_ρ can be written

$$dF_\rho(\tilde{\rho};\boldsymbol{x},t) = f_\rho(\tilde{\rho};\boldsymbol{x},t)d\tilde{\rho} \ . \tag{2.3}$$

Let $Z_r(\tilde{\rho};\boldsymbol{x},t)$ be the height of a fluid element with density $\tilde{\rho}$ in the minimum potential energy state. Recall that in the state of lowest potential energy, the fluid has settled so that the lightest fluid is on top. If the fluid column has height H then $Z_r(\tilde{\rho};\boldsymbol{x},t)/H$ is the fraction of fluid having density greater than $\tilde{\rho}$, i.e.,

$$Z_r(\tilde{\rho};\boldsymbol{x},t) = H[1 - F(\tilde{\rho};\boldsymbol{x},t)] \ . \tag{2.4}$$

Tseng and Ferziger [2001] show the equivalence between the sorting and PDF approaches to defining background potential energy from which it is concluded that

$$\Phi_b(\tilde{\rho};\boldsymbol{x},t) = \frac{H\tilde{\rho}(\boldsymbol{x},t)}{\pi_1 F^2}[1 - F_\rho(\tilde{\rho};\boldsymbol{x},t)] \ . \tag{2.5}$$

These are functions of a random variable. Evaluating them depends on f_ρ, and therefore F_ρ being known. For a simulated flow, one approach is to replace f_ρ with the normalized histogram determined by sampling a given volume and taking care, e.g., by assuming a cylindrical volume, to eliminate any spatial dependence from f_ρ (c.f. [Tseng and Ferziger, 2001]).

Alternatively, consider a density field that is known analytically. Then (2.5) may be evaluated using the methods of random variables. To illustrate the approach, let density be homogeneous in x and y, omit the time dependence from the notation, and let $\tilde{z} \in [0...H)$ be a uniformly distributed random variable. Further, let

$$\tilde{\rho} = g(\tilde{z})$$

and $g' = dg(\tilde{z})/d\tilde{z}$. If the density field is in its settled state at all times, $\tilde{\rho}$ decreases monotonically with increasing height and, for a specific value of $\tilde{\rho}$, $\tilde{\rho} = g(\tilde{z})$ has exactly one solution for $\tilde{z} \in [0...\pi)$. Denote this solution as $\tilde{z}_1$. Then from Papoulis [1965],

$$f_\rho(\tilde{\rho}) = \frac{1}{\pi \left| g'(\tilde{z}_1) \right.} \ . \tag{2.6}$$

Increasingly more complex cases can be considered, the next simplest being one in which $\tilde{\rho} = g(\tilde{z})$ has two solutions, $\tilde{z}_1$ and $\tilde{z}_2$, for some value of $\tilde{\rho}$. Then

$$f_\rho(\tilde{\rho}) = \frac{1}{\pi \left| g'(\tilde{z}_1| \right.} + \frac{1}{\pi \left| g'(\tilde{z}_2| \right.} \ . \tag{2.7}$$

From (2.6) and (2.7) it may be correctly surmised that this approach can be generalized to any function $g(\tilde{z})$, as proved in [Papoulis, 1965] (c.f.[Holliday and McIntyre, 1981]).

2.1.1 Exact and Implied Equations for Background and Available Potential Energy for Boussinesq Fluid

By definition background potential energy is given by $\hat{\Phi}_b = \hat{Z}_* \hat{\rho} \hat{g}$ where Z_* is the height of a fluid element in the lowest energy state. Energy is non-dimensionalized by $\hat{\rho}_0 \hat{V}^2$, and $\Phi = \hat{\Phi}/\hat{\rho}_0 \hat{g} \hat{L} \mathrm{F}^2 \pi_1$. Following the same approach as in §1.2.2, we get the the non-dimensional equation for background potential energy:

$$\frac{D\Phi_b}{Dt} = \frac{1}{\pi_1 \mathrm{F}^2} \left[Z_* \frac{\partial \rho}{\partial t} + \rho \frac{\partial Z_*}{\partial t} \right]$$

Note that the reference height, Z_*, is constant in time. Hence $\partial Z_*/\partial t = 0$. From (1.4), (2.5), (1.10c) we can simplify the above relation to,

$$\frac{D\Phi_b}{Dt} = -\frac{Z_* \nabla^2 \theta}{\mathrm{Pr\ Re\ F}^2} \tag{2.8}$$

A similar equation for available potential energy can be derived by using (1.11c), (2.8) and definition of available potential energy, $\hat{\Phi}_a = \hat{\rho} \hat{g} (\hat{z} - \hat{Z}_r)$:

$$\frac{D\Phi_a}{Dt} = \quad -\frac{z \nabla^2 \theta}{\mathrm{Pr\ Re\ F}^2} + \frac{Z_* \nabla^2 \theta}{\mathrm{Pr\ Re\ F}^2} \quad + \frac{w}{\pi_1 \mathrm{F}^2} - \frac{\theta w}{\mathrm{F}^2} \tag{2.9}$$

The second term in the right hand side of (2.9) is the same as the diffusion term in (2.8). This term (ϕ_d), represents the rate of exchange between background and available potential energy as a result of diffusion, which is analogous to dissipation rate of kinetic energy as mentioned in chapter 1. Third and fourth terms in (2.9) represent the rate of exchange between potential and internal energy possibly as a result of pressure work and exchange with kinetic energy via buoyancy flux (ϕ_z).

Following the expansion as in §1.2.3 that lead to (1.12), we expand (2.8) and (2.9) and retain only the lowest order terms, π_1 and π_2,

$$\frac{D\Phi^{0,0}}{Dt} = -\frac{z\nabla^2\theta^{0,0}}{\mathrm{Pr\ Re\ F^2}} - \frac{\theta^{0,0}w^{0,0}}{\mathrm{F^2}}, \tag{2.10a}$$

$$\frac{D\Phi_b^{0,0}}{Dt} = -\frac{Z_*\nabla^2\theta^{0,0}}{\mathrm{Pr\ Re\ F^2}}, \tag{2.10b}$$

$$\frac{D\Phi_a^{0,0}}{Dt} = -\frac{z\nabla^2\theta^{0,0}}{\mathrm{Pr\ Re\ F^2}} + \frac{Z_*\nabla^2\theta^{0,0}}{\mathrm{Pr\ Re\ F^2}} - \frac{\theta^{0,0}w^{0,0}}{\mathrm{F^2}}\ . \tag{2.10c}$$

As a result of the expansion, only the terms that can be computed in a simulation are retained in (2.10), which can be used along with (1.13) to thoroughly understand the dynamics of potential energy in a Boussinesq fluid and formulate an energy budget.

CHAPTER 3

ANALYTICAL PROOFS OF CONCEPT

Simple analytical problems provide a framework for understanding the dynamics of available and background potential energies and, in particular, the flux of each through the boundaries of a hypothetical domain. To simplify the notation of §1.2, the superscripts related to the power series expansions are dropped so that, e.g., $\theta = \theta(\boldsymbol{x}, t) = \theta^{0,0}$ is the temperature that obeys (1.10c). Note that the energies are relative to arbitrary reference values taken to be zero.

Even though our primary interest is in local values of energy, it is important to understand energy balance locally as well as globally. While K, U and Φ represent local values of kinetic, internal and potential energy respectively; the box average for the volume is indicated by '$(\ )_{avg}$', e.g. K_{avg} is the kinetic energy averaged over the volume. We consider two analytical cases, which are summarized in the following table.

Table 3.1. An Overview of Analytical Examples

Example	Boundary Conditions	Observations
1	Settled fluid in an adiabatic rigid box with no mass flux. $\Phi_t = \Phi_b,\ \Phi_a = 0.$	Background potential energy in the box increases with time due to molecular diffusion
2	Unsettled fluid in a rigid box with equal and opposite mass fluxes at top and bottom. $U_{avg} = 0, K_{avg} = 0.$	Potential energy increases at the expense of energy outside the box.

3.1 Example 1: Adiabatic Box

Let us first consider a simple example of an adiabatic box with $z \in [0, \pi)$, with the fluid at the top and bottom surface maintained at different temperatures. The initial velocity is zero and the initial temperature field is not constant but cannot be rearranged to a lower potential energy state. Therefore there is no available potential energy and no kinetic energy at any time. We can see from Figure 3.1 that diffusive mixing allows the density to settle into a uniform profile over time. The choice of diffusion rate is arbitrary and so $\pi_2 \mathrm{PrRe}$ is taken to be unity:

Initial Conditions:	$\theta(\boldsymbol{x}, 0) = -\cos z$
	$\boldsymbol{v}(\boldsymbol{x}, 0) = \{0, 0, 0\}$
Boundary Conditions:	periodic in x, y
	$\partial\theta/\partial z\|_{\theta=0} = 0$
	$\partial\theta/\partial z\|_{\theta=\pi} = 0$
Temperature:	$\theta(\boldsymbol{x}, t) = -\cos(z)\exp(-t)$
Density:	$\rho(\boldsymbol{x}, t) = 1 + \pi_1 \cos(z)\exp(-t)$
Kinetic Energy:	$K(\boldsymbol{x}, t) = 0$
	$K_{avg}(t) = 0$
Internal Energy:	$U(\boldsymbol{x}, t) = -\frac{1}{\pi_2 \gamma}\cos(z)\exp(-t)$
	$U_{avg}(t) = 0$
Potential Energy:	$\Phi(\boldsymbol{x}, t) = \frac{1}{\pi_1 \mathrm{F}^2} z\left[1 + \pi_1 \cos(z)\exp(-t)\right]$
	$\Phi_{avg}(t) = \frac{1}{\pi_1 \mathrm{F}^2}\left[\frac{\pi^2}{2} - 2\pi_1 \exp(-t)\right]$

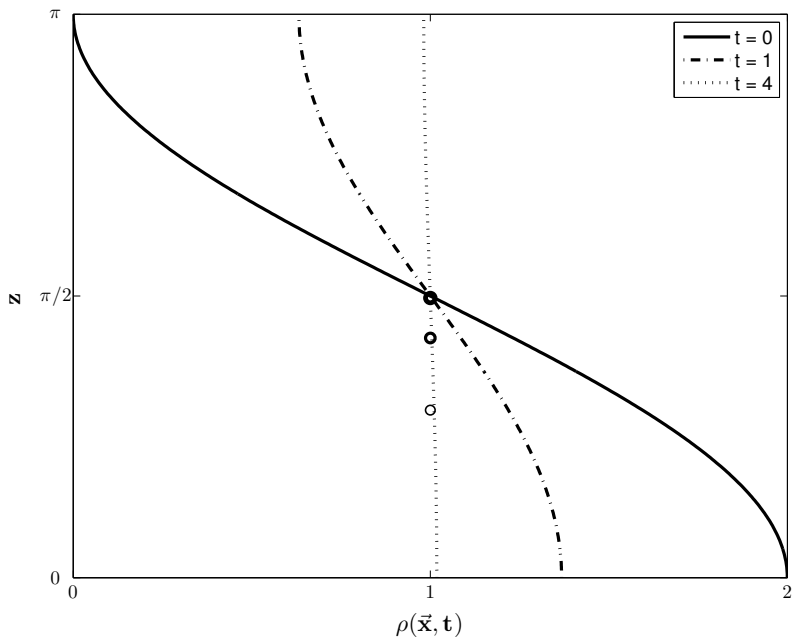

Figure 3.1. Density profile in a hypothetical domain at times t=0, 1, 4. Position of center of gravity is shown by circles, getting darker as time progresses.

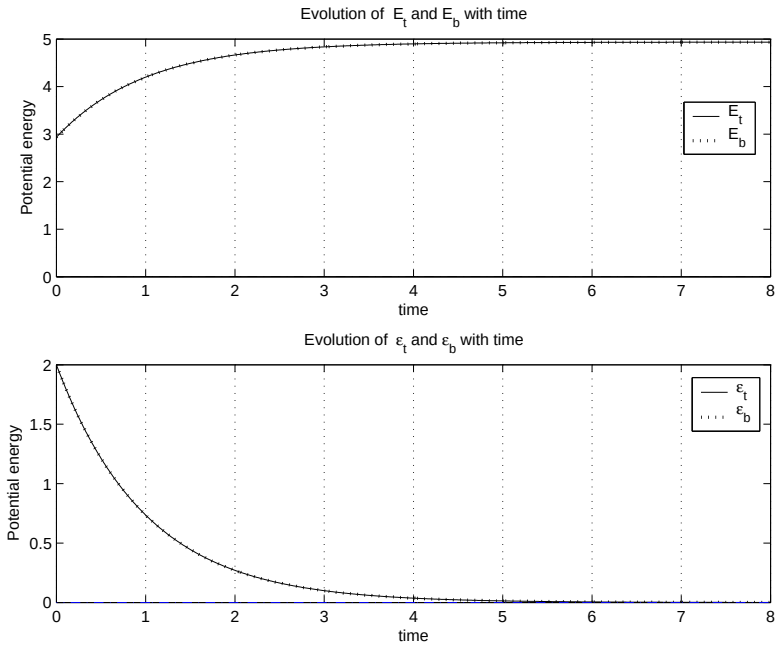

Figure 3.2. a) Change in Total (E_t) and Background (E_b) Potential Energy with time. b) Time rate of change of Potential Energy ($\varepsilon_t, \varepsilon_b$)

In the absence of any change in kinetic energy, the total potential energy in the box increases with time (see Figure 3.2). From inspection, $\rho(\boldsymbol{x}, t)$ is always in the settled configuration and so the background potential energy is equal to the total potential energy and the available potential energy is equal to zero. To demonstrate the approach described in chapter 2 for this simple case, write

$$\tilde{\rho} = 1 + \pi_1 \cos(\tilde{z}) \exp(-t) \ , \quad \tilde{z} \in [0...\pi)$$

and solve for $\tilde{z}$ in terms of $\tilde{\rho}$:

$$\tilde{z} = \arccos\left(\frac{\tilde{\rho} - 1}{\pi_1 \exp(-t)}\right) \ .$$

Then from (2.6),

$$f_\rho(\tilde{\rho}) = \frac{1}{\pi\sqrt{[\pi_1 \exp(-t)]^2 - [\tilde{\rho} - 1]^2}}$$

and

$$F_\rho(\tilde{\rho}) = \frac{1}{\pi}\left\{\frac{\pi}{2} + \arctan\left[\frac{\tilde{\rho} - 1}{\sqrt{[(\pi_1 \exp(-t)]^2 - [\tilde{\rho} - 1]^2}}\right]\right\} = \frac{1}{\pi}\left(\pi - \tilde{z}\right) \ .$$

From (2.5)

$$\Phi_b = \frac{1}{\pi_1 \mathrm{F}^2} z \left[1 + \pi_1 \cos(z) \exp(-t)\right] \ ,$$

which is exactly what is expected given that $\Phi_b = \Phi$ for this case.

The boundary conditions are such that there is not heat and mass transfer at the bounding surfaces. Therefore we can apply the zero velocity and the boundary conditions to (1.13) and analyze the energy budget of the box as follows.

Kinetic Energy:	$\frac{D}{Dt}K = \ 0$	$\frac{D}{Dt}K_{avg}\vert_{t=0} = 0$
Internal Energy:	$\frac{D}{Dt}U = \ \frac{\cos(z)\ e^{-t}}{\mathrm{Pr\ Re}\ \pi_2}$	$\frac{D}{Dt}U_{avg}\vert_{t=0} = 0$
Potential Energy:	$\frac{D}{Dt}\Phi = \ \frac{-z\ \cos(z)\ e^{-t}}{\mathrm{Pr\ Re\ F^2}}$	$\frac{D}{Dt}\Phi_{avg}\vert_{t=0} = \pi$
Energy Budget:	$\frac{D[K+U+\Phi]}{Dt} = \left[\frac{1}{\pi_2} - \frac{z}{\mathrm{F^2}}\right]\frac{\cos(z)\ e^{-t}}{\mathrm{Pr\ Re}}$	$\frac{D[K+U+\Phi]_{avg}}{Dt}\vert_{t=0} = \pi$

As we can see from the above equations, the energy does not balance. If we let $(\,)'$ indicate a material derivative, the cumulative imbalance in the energy budget for this simple case is $\Phi' - U' = \pi$ at time $t = 0$. For energy to be conserved in the box, the potential energy should increase at the expense of internal energy. From the energy budget in the above table it is clear that all the changes in energies will add up to zero only if $\pi_2 = F^2$. Therefore, the condition $\pi_2 = \mathrm{F}^2$ is necessary for energy conservation.

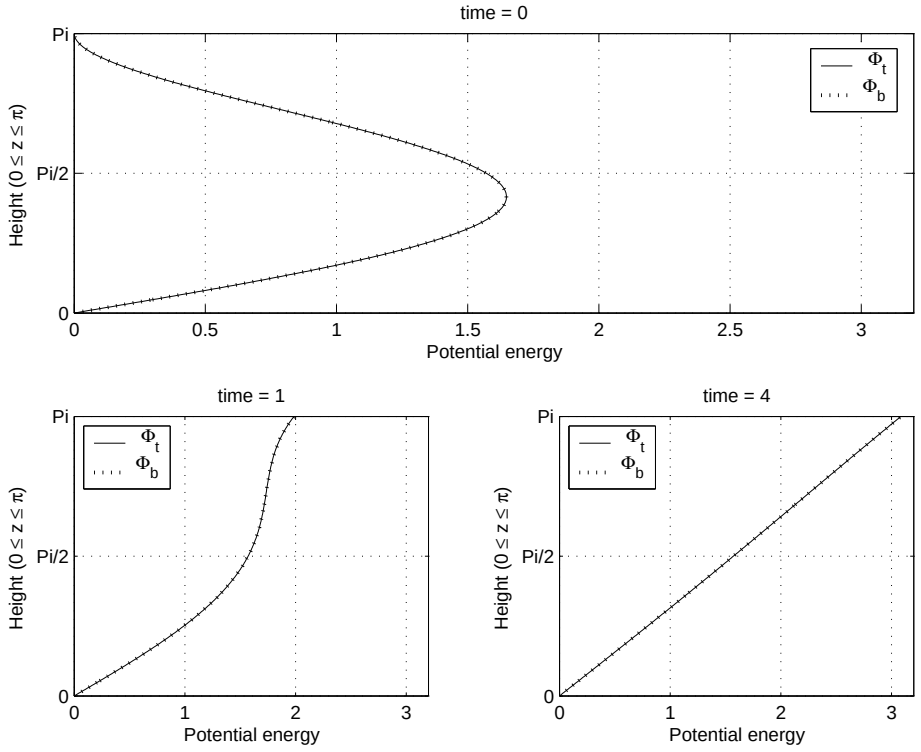

Figure 3.3. Distribution of potential energy in the control volume at times, t=0, 1, 4.

Physical Interpretation: In absence on vertical velocity w, there is no exchange of potential energy with kinetic energy via buoyancy flux and with internal energy via pressure work. Net effect of diffusion in the box is zero as the entire mass of fluid remains in the box at all times. However, potential energy of the box is increasing as a result of exchange with internal energy at a rate (ϕ_i), which is a result of Boussinesq equation of state as discussed in chapter 2. ϕ_i is the result of rearrangement of mass

inside the box which, leads to an increase in potential energy. But since we do not allow the box to expand or contract (non-divergent velocity), corresponding change in internal energy is zero as there is no pressure work. Hence energy is not conserved. There is no available potential energy is present in the box, hence $\phi_d = \phi_i$, both ϕ_i and ϕ_d can be calculated exactly. Hence energy or mass is not conserved locally and energy is not conserved over the volume.

3.2 Example 2: Box with mass flux at top and bottom

Consider a box with $z \in [0, 2\pi)$. There in is no initial velocity, hence the initial kinetic energy in the box is zero. Also the interaction between kinetic and internal energy can be ignored. However, the initial temperature is not statically stable and can be arranged to a lower energy state. The boundary conditions allow equal but opposite flux of mass at the top and the bottom such that total mass is conserved. Again, the choice of diffusion rate is arbitrary, hence $\pi_2 \mathrm{PrRe}$ are taken to be unity.

Initial Conditions:	$\theta(\boldsymbol{x}, 0) = -\sin z$
	$\boldsymbol{v}(\boldsymbol{x}, 0) = \{0, 0, 0\}$
Boundary Conditions:	periodic in x, y
	$\partial\theta/\partial z\|_{z=0} = 1 \cdot \boldsymbol{n}$
	$\partial\theta/\partial z\|_{z=2\pi} = 1 \cdot \boldsymbol{n}$
Temperature:	$\theta(\boldsymbol{x}, t) = -\sin(z)\exp(-t)$
Density:	$\rho(\boldsymbol{x}, t) = 1 + \pi_1 \sin(z)\exp(-t)$
Kinetic Energy:	$K(\boldsymbol{x}, t) = 0$
	$K_{avg}(t) = 0$
Internal Energy:	$U(\boldsymbol{x}, t) = -\frac{1}{\pi_2 \gamma}\sin(z)\exp(-t)$
	$U_{avg}(t) = 0$
Potential Energy:	$\Phi(\boldsymbol{x}, t) = \frac{1}{\pi_1 \mathrm{F}^2} z\,[1 + \pi_1 \sin(z)\exp(-t)]$
	$\Phi_{avg}(t) = \frac{1}{\pi_1 \mathrm{F}^2}\,[(2\pi^2) - 2\pi\pi_1 \exp(-t)]$

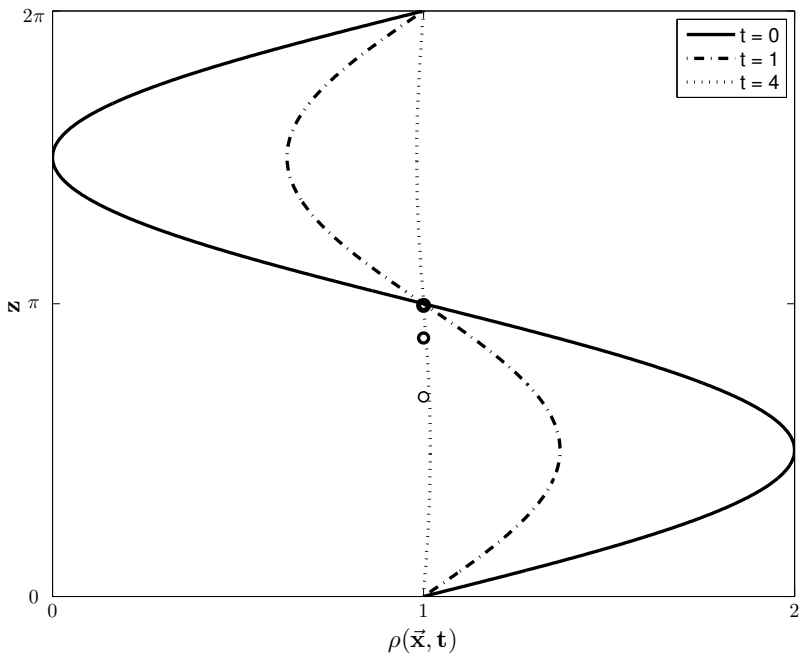

Figure 3.4. Density profile in a hypothetical domain at times t=0, 1, 4. Position of center of gravity is shown by circles, darkest at t = 4

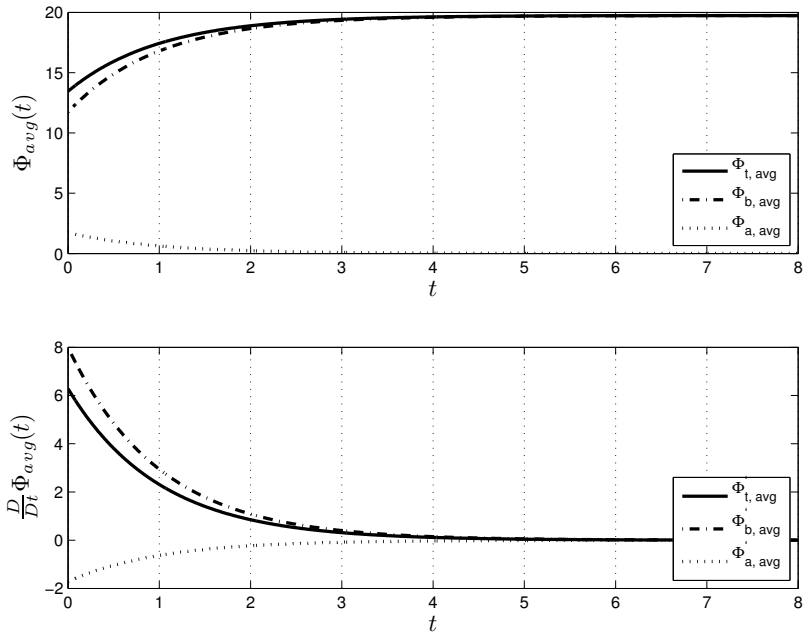

Figure 3.5. a) Change in Total, Available and Background Potential Energy with time. b) Time rate of change of Potential Energy

This example is more insightful as there is a finite available potential energy in the control volume and mass flux at the bounding surfaces initially. APE and fluxes contribute to the energy budget and help us better understand the dynamics of energy in diffusive mixing.

Following the approach in chapter 2,

$$\tilde{\rho} = 1 + \pi_1 \sin(\tilde{z}) \exp(-t) \ , \quad \tilde{z} \in [0...2\pi)$$

and $\tilde{z}$ in terms of $\tilde{\rho}$:

$$\tilde{z} = \arcsin\left(\frac{\tilde{\rho} - 1}{\pi_1 \exp(-t)}\right) \ .$$

Then from (2.6),

$$f_\rho(\tilde{\rho}) = \frac{2}{\pi\sqrt{[\pi_1 \exp(-t)]^2 - [\tilde{\rho} - 1]^2}}$$

and

$$F_\rho(\tilde{\rho}) = \frac{2}{\pi}\left\{\arctan\left[\frac{\tilde{\rho} - 1}{\sqrt{\left[(\pi_1 \exp(-t)\right]^2 - \left[\tilde{\rho} - 1\right]^2}}\right]\right\} = \frac{2}{\pi}\left(\pi - \tilde{z}\right) \ .$$

From (2.5)

$$\Phi_b = \frac{1}{\pi_1 \mathrm{F}^2}(\pi - 2\tilde{z})\left[1 + \pi_1 \sin(\tilde{z}) \exp(-t)\right] \ ,$$

and

$$\Phi_a = \frac{1}{\pi_1 \mathrm{F}^2}(3\tilde{z} - \pi)\left[1 + \pi_1 \sin(\tilde{z}) \exp(-t)\right] .$$

Mixing allows the fluid in the box to settle to the lowest energy state over the time. Available potential energy is converted to background potential energy at a rate ϕ_d, due the changes in the density, or in other words as a result of diapycnal mixing. Ideally, the total potential energy in the box should be constant. Energetics

of the box can be analyzed by following (1.13) as we did for the adiabatic box in Example 1. Results are listed in the following table.

Kinetic Energy:	$\frac{D}{Dt}K = 0$	$\frac{D}{Dt}K_{avg} = 0$
Internal Energy:	$\frac{D}{Dt}U = \frac{\sin(z)\ e^{-t}}{\mathrm{Pr\ Re}\ \pi_2}$	$\frac{D}{Dt}U_{avg} = 0$
Potential Energy:	$\frac{D\Phi}{Dt} = \frac{-e^{-t}z\sin(z)}{\mathrm{Pr\ Re\ F^2}}$	$\frac{D}{Dt}\Phi_{avg} = 2\pi$
Energy Budget :	$\frac{D[K+U+\Phi]}{Dt} = \left[\frac{1}{\pi_2} - \frac{z}{\mathrm{F^2}}\right]\frac{\sin(z)\ e^{-t}}{\mathrm{Pr\ Re}}$	$\frac{D[K+U+\Phi]_{avg}}{Dt}\vert_{t=0} = 2\pi$

From Figure 3.5 and the above table notice that total potential energy is increasing with time. Analysis of available potential energy using (2.9), as shown in Figure 3.5, puts forth a very interesting situation.

$$\Phi_t': \qquad + \underbrace{-e^{-t}\ z\ \sin(z)}_{S_{diff}}$$

$$\Phi_b': \quad + \overbrace{(-\pi + \mathrm{arccot}\left[\frac{|\cos(z)|}{\sin(z)}\right]\sin(z))\ e^{-t}}^{\boldsymbol{\phi_d}}$$

$$\Phi_a': \quad - \overbrace{(-\pi + \mathrm{arccot}\left[\frac{|\cos(z)|}{\sin(z)}\right]\sin(z))\ e^{-t}}^{\boldsymbol{\phi_d}} \quad + \underbrace{-e^{-t}\ z\ \sin(z)}_{S_{diff}}$$

It is clear that the while available potential energy is converted to background potential energy due to mixing (ϕ_d), it is simultaneously increasing with time as a result of diffusive heat and mass transfer across the bounding surfaces (S_{diff}, surface diffusion), thus increasing the total potential energy. We can exactly calculate the change in potential energy due to diffusive fluxes and mixing. Hence the potential energy balance is achieved locally as well as over a control volume.

Physical Interpretation: From inspection of $\rho(\boldsymbol{z}, t)$, it is clear that the total density in the box over time remains constant. In a Boussinesq fluid volume is conserved. The box is gaining energy via external fluxes and in turn increasing the total

potential energy. If we treat the box as a fluid parcel of constant mass, increase in potential energy indicates that the fluid parcel is rising with respect to the surrounding fluid.

3.3 Discussion of Energy Equations

Consideration of the exact (1.12) and implied (1.13), (2.10) energy equations for a Boussinesq fluid leads to several significant observations. In Example 1 of chapter 3 we consider energy conservation for a rigid control volume with no surface fluxes. This reveals the requirement that $F^2 = \pi_2$, or $\hat{g}\hat{L} = \hat{C}_p/\hat{\alpha}$, for strict energy conservation in a rigid adiabatic control volume. This requirement is a consequence of the equation of state. Alternatively, by the analysis of Winters et al. [1995], molecular diffusion results in a transfer of internal energy to potential energy. In the absence of isothermal compressibility (β), either heat or mass flux must occur at the boundary of a rigid control volume in order for energy to be conserved.

The diffusion terms involving $\theta^{1,0}$ and $\theta^{0,1}$ cannot be computed. Unless the gradients of these higher order terms are very large, the diffusion they represent will be small compared with that due to gradients in $\theta^{0,0}$, which can be computed. It is assumed that the higher order diffusion terms are negligible and that, since diffusion is conservative, they result, at worst, in errors in the spatial location of internal energy. The diffusion terms involving $\theta^{0,0}$ result in energy not being conserved except in the special case of $F^2 = \pi_2$. The error can be computed, though, and so at least the energy budget can be numerically balanced as energy conversions can be accounted for, as shown in chapter 3.

The term $w/(\pi_1 \mathrm{F}^2)$ in (1.11) also warrants some physical interpretation. This term appears when the thermodynamic and hydrostatic pressures are combined and represents transfer from internal to potential energy. It can be interpreted as pressure work resulting from velocity divergence working against the hydrostatic pressure

gradient. Perhaps more intuitively, though, if a fluid element has positive vertical velocity then it will move upward and gain potential energy. It will also expand due to the lower hydrostatic pressure and lose internal energy.

Winters et al. [1995] consider energy balances in control volumes, not local balances, and determine that this effect irreversibly converts internal energy to potential energy. We conclude that, in the differential Boussinesq energy equations, coupling between potential and internal energies is not straightforward to compute. The associated terms do not even appear in the implied equations and in the exact equations take the form $z\nabla \cdot \boldsymbol{v}^{1,0}/\mathrm{F}^2$ and $(w^{0,0} + \pi_1 w^{1,0})/\pi_1 \mathrm{F}^2$. These terms can be computed since $\boldsymbol{v}^{1,0}$ can be determined from (1.10a) and (1.10c).

The loss of energy due to viscous dissipation as seen in (1.11d), has not been simulated in the two examples discussed above, as velocity has been restricted to zero in either of the cases. However, this effect can be computed in terms of $\boldsymbol{v}^{0,0}$, that is, in terms of known quantities. It can be accounted for and presents no difficulty in studying the energetics of a Boussinesq fluid.

CHAPTER 4

TEST OF NUMERICAL METHODS FOR PARTITIONING POTENTIAL ENERGY

Analytical examples in chapter 3 help us understand the energetics of diffusive mixing in 1D simulations. They act as a base to build progressively complex simulations in two and three dimensions. The primary purpose of the analytical examples is to validate the PDF approach (chapter 2) in the numerical implementation. For the purpose of validation, we have numerically solved the problem in Example 2 in which, the density profile is sinusoidal.

4.1 Density Field

First step in the process is to create a grid of points in a control volume where the values of density are known. In Boussinesq approximation, the temperature and density are related by using the equation of state in (1.4). As we are solving a diffusive problem, the temperature field is obtained by solving the heat equation,

$$\frac{\partial \theta}{\partial t} = \frac{1}{\mathrm{PrRe}} \nabla^2 \theta, \tag{4.1}$$

and by applying periodic boundary conditions (see chapter 3, example 2 for details). Solution to (4.1) will give a temperature $\theta(\boldsymbol{x}, t)$. In this 1D case,

$$\theta(z, t) = -\sin z \ \exp -t.$$

From (1.4),

$$\rho(z, t) = 1 + \sin z \exp -t.$$

We start with density ($\tilde{\rho}$) at random locations in the control volume. In a 1D problem, $\tilde{\rho} = \rho(\tilde{z}, t)$, where $\tilde{z}$ is uniformly distributed random variable, equivalent to height z in probability sample space. If M is total number of points, then $\tilde{z}$ and eventually $\tilde{\rho}$ will be calculated at M random locations in the sample space. Thus we have a density field in the z direction.

4.2 Potential Energy

Density field at a particular time, say t_0, is known, the next step is to compute the total and background potential energy of the fluid. Total potential energy (TPE) is fairly easy to compute, since we already have the density (ρ) relative to vertical height z. However, in order to compute background potential energy, z_* (height of every particle in the reference state) needs to be known.

TPE (ϕ_t)	BPE (ϕ_b)(?)
$\tilde{\rho_1} \rightarrow \tilde{z_1}$	$\tilde{\rho_1} \rightarrow z_{*1}(?)$
$\tilde{\rho_2} \rightarrow \tilde{z_2}$	$\tilde{\rho_2} \rightarrow z_{*2}(?)$
$\tilde{\rho_3} \rightarrow \tilde{z_3}$	$\tilde{\rho_3} \rightarrow z_{*3}(?)$

As discussed in chapter 2, z_* of a fluid parcel depends on the state of all the surrounding parcels. Therefore z_* is obtained from the cumulative density function (CDF) of the entire density field by following the relation,

$$dF_\rho(\tilde{\rho}; \boldsymbol{x}, t) = f_\rho(\tilde{\rho}; \boldsymbol{x}, t) d\tilde{\rho} \ .$$

In turn the vertical position of a fluid particle in a reference state is computed (from (2.4)). Local background potential energy of each parcel is then computed using the relation (2.5).

BPE (ϕ_b)		
$\tilde{\rho}_1$	$\rightarrow$	$H[1 - F_\rho(\tilde{\rho}_1)]$
$\tilde{\rho}_2$	$\rightarrow$	$H[1 - F_\rho(\tilde{\rho}_2)]$
$\tilde{\rho}_3$	$\rightarrow$	$H[1 - F_\rho(\tilde{\rho}_2)]$

4.3 PDF by sorting

A probability density function (PDF) may be approximated by dividing the range of values of a random variable into bins. One can measure the *frequency* of occurrence of different values (range of values) and get a fair idea about the distribution of a random variable. 'Bin size' is the range of values that come under each bin. Hence smaller bin size leads to more number of bins required to divide a sample space and vice versa. The process of dividing a sample space into bins is called *discretizing*.

While computing background potential energy from a CDF of the density, Tseng and Ferziger [2001] employ adaptive mesh to improve accuracy. Adaptive mesh is a term used if a mesh adjusts automatically based to the distribution of the variable. In the more general sense, the program analyzes the density gradient and depending on the steepness of the gradient, adjusts the bin size. So that the mesh is finer where the density gradient is steep.

Our approach to discretizing is just taking the adaptive mesh to its logical limit. Instead of changing the bin size based on distribution, every value of a random variable is assigned to a new bin i.e. "one bean in each bin". This is achieved by sorting the density field. If M is the total number of samples, the probability of occurrence of each value is therefore, $1/M$. In other words each bin has the same frequency and computing the PDF is equivalent to sorting the density field. By sorting it is possible to directly compute the CDF of density and in turn calculate the background potential energy. Also the computational effort associated with integrating the PDF (in order to compute a CDF) is saved.

4.4 Results

The diffusion problem is solved analytically in §3.2 and numerically by following the sorting approach to compute the CDF of the density field. It should be noted that in §3.2 the PDF of density ($\tilde{\rho}$) was computed analytically and then integrated to get the cumulative distribution. In the sorting approach the cumulative distribution is computed for $M = 128$ points. This numerical approximation and the analytically computed (exact) CDF are compared in Figure 4.1. As we can see from the figure the approximation by sorting is identical to the exact analytically computed CDF.

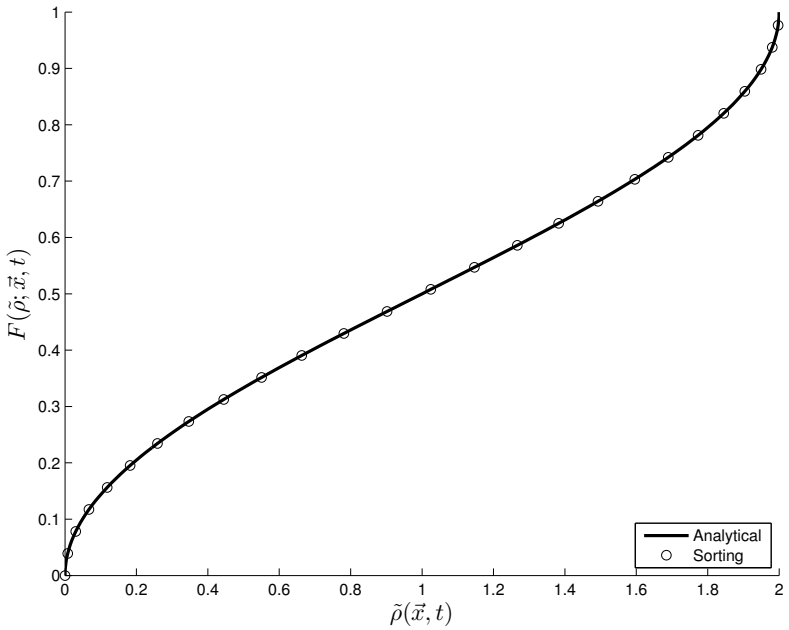

Figure 4.1. Cumulative Density Function (CDF) computed by Analytical approach vs. Sorting

While analyzing the accuracy of the sorting approach we have assumed the values from §3.2 to be *exact*, hence the term *error* merely represents the difference in the results of the two methods.

$$\text{error} = \phi_b(z,t)_{(analytical)} - \phi_b(z,t)_{(sorting)}.$$

The l_2 norm of the error in background potential energy vs number of points (M) is shown in Figure 4.2.

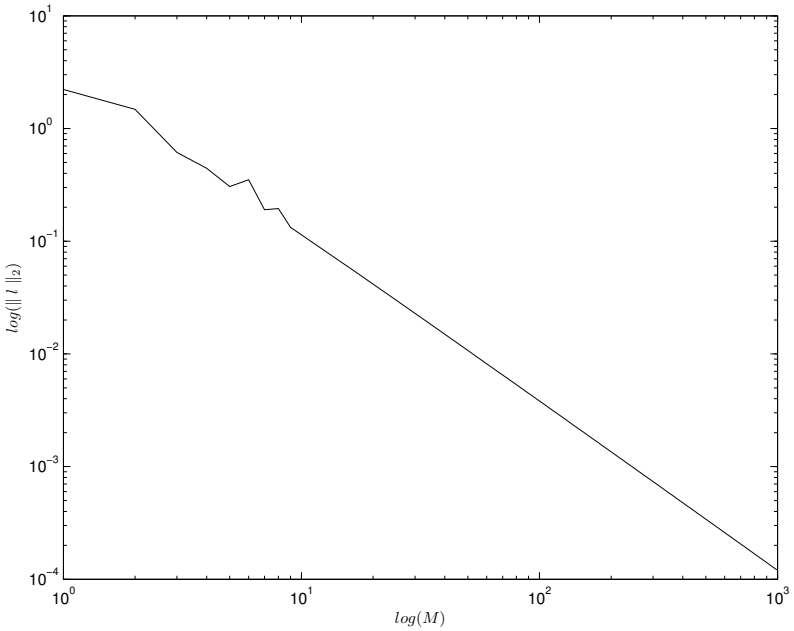

Figure 4.2. Log-Log plot of number of sample points vs. l_2 of error in background potential energy using sorting method

As we can see from Figure 4.2, our sorting approach is very accurate in computing background potential energy and the cumulative error falls below 0.1% when more than 260 points are used in the z direction. Note that the error plot is a straight line with a slope of -1. Therefore,

$$\log l_2 = -1 \log M + \log C$$

and

$$l_2 = CM^{-1}.$$

Hence the error in background potential energy converges as M^{-1} (first order method).

Sorting approach is robust and can be applied to any case irrespective of our ability to compute and invert the analytical density function as is required in the analytical approach. However, when this approach is applied to 3-D simulations, the advantages of the sorting approach are overshadowed by the errors in available potential energy resulting from descritization.

CHAPTER 5

AMBIENT AND DEVIATORIC POTENTIAL ENERGY

As discussed in chapters 3 and 4, the stochastic approach [Tseng and Ferziger, 2001] is very accurate in computing the available potential energy both analytically and numerically. In this approach, the reference height of a fluid parcel is approximated from the probability density function of the densities of all the fluid parcels in the control volume.

In the numerical implementation of this approach (chapter 4), it is clear that the error in the available potential energy depends on the vertical (z) descritization or in case of sorting, it depends on the number of samples in the vertical direction. The error resulting from descritization is compounded as we consider more complex 2-D and 3-D problems. This is because the number of samples in a horizontal layer are the multiples of x and y descritization instead of a single sample in each horizontal layer as considered in the previous 1-D examples. As a result the advantages of the stochastic approach in terms of the numerical accuracy are overshadowed by the errors resulting from descritization. This has motivated us to compute the background and available potential energies in terms of density fluctuations and vertical displacement [Holliday and McIntyre, 1981]. In the following sections, we define ambient and deviatoric potential energies as surrogates to background and available potential energies in viscous fluids. Furthermore, the potential energies and their surrogates are compared using direct numerical simulations in chapter 6

In an ideal fluid, the background potential energy of a fluid parcel does not change and so the settled state defined by Lorenz is persistent. The available potential energy

Φ_a can be computed in terms of the density fluctuations about the persistent state [Holliday and McIntyre, 1981]. The same method can be applied to viscous fluids to compute a deviatoric potential energy $\Phi_a^*(\boldsymbol{x}, t)$ in terms of the density fluctuations about the persistent ambient density rather than the time-varying settled density. Then $\Phi_a^*(\boldsymbol{x}, t)$ is the difference between the total potential energy and the ambient potential energy $\Phi_b^*(\boldsymbol{x}, t)$.

The deviatoric potential energy is an attractive quantity for several reasons. The first follows from the observation made in the introduction of this chapter that some practical flows have a quasi-persistent background state and so Φ_a^* can provide interesting information about the flow dynamics. A second attractive feature of Φ_a^* is that it is differentiable to the extent that the ambient density field is differentiable. This means that very precise local energy balances can be computed, including the local irreversible rate of conversion of Φ_a^* to Φ_b^*. In contrast, when Φ_a is computed, significant numerical error may be introduced due to the discretization.

A third, and related, reason to consider Φ_a^* instead of Φ_a is that neither mass nor energy is conserved locally in a Boussinesq fluid, as discussed in chapter 1. The facts that a Boussinesq fluid does not exactly obey the laws of physics and that the numerical error in Φ_a can be expected to be much larger than that in Φ_a^* leads to the question of whether Φ_a or Φ_a^* is the more useful quantity for understanding the dynamics of the fraction of potential energy available for conversion to kinetic energy.

Winters et al. [1995] derive dynamic equations for the integral of Φ_b and Φ_a over a control volume, but the integrands are not the Eulerian energies. To identify these, define $\rho_*(\boldsymbol{x}, t)$ as the settled density field and $z_*(\boldsymbol{x}, t)$ as the vertical position in the settled state of the fluid parcel at position $(\boldsymbol{x}, t)$. When the density field settles to its lowest energy state, the fluid parcel at $(\boldsymbol{x}, t)$ moves a vertical distance $\zeta = z - z_*$. By the analysis of Holliday and McIntyre [1981], the available potential energy at $(\boldsymbol{x}, t)$ is

$$\Phi_a(\boldsymbol{x},t) = \frac{1}{2\pi_1 F^2}\zeta(\boldsymbol{x},t)\rho_e(\boldsymbol{x},t), \tag{5.1}$$

where $\rho_e(\boldsymbol{x},t) = \rho(\boldsymbol{x},t) - \rho_*(\boldsymbol{x},t)$ is the excess density relative to the sorted state. The available potential energy averaged over a volume $\forall$ is,

$$\langle\Phi_a\rangle = \frac{1}{2\pi_1 F^2}\left[\int_{\forall}\zeta\rho\ d\forall - \int_{\forall}\zeta\rho_*\ d\forall\right]\ . \tag{5.2}$$

Since the energy liberated by moving a fluid parcel from the unsorted state to the sorted state is equal to that required to move it from the sorted to the unsorted state, the two integrals in the preceding equation have equal magnitudes but opposite signs so that the expression for $\langle\Phi_a\rangle$ derived by Winters et al. [1995] is recovered. If the fluid is ideal then the sorted state is time-invariant. In this case, $\Phi_a(\boldsymbol{x},t)$ can be written in terms of a series expansion in terms of ρ_* and ρ_e, as done by Holliday and McIntyre [1981].

Now consider a flow with a persistent ambient temperature, $\overline{\theta}(z)$. Then the temperature can be decomposed as

$$T = T_0 + \overline{\theta}(z) + \theta'(\boldsymbol{x},t)\ , \tag{5.3}$$

where $\theta'(\boldsymbol{x},t)$ is the deviatoric temperature. Applying the decomposition to (1.10c) yields a trivial equation for temporal evolution of ambient temperature plus an equation for the deviatoric temperature that can be solved with periodic boundary conditions. Alternatively, the latter can be written in terms of the deviatoric density $\rho'(\boldsymbol{x},t)$ so that the flow is described by the set of equations

$$\nabla\cdot\boldsymbol{v} = 0 \tag{5.4a}$$

$$\frac{D\boldsymbol{v}}{Dt} = -\nabla p' + \frac{1}{\mathrm{Re}}\nabla^2\boldsymbol{v} - \frac{1}{\mathrm{F}^2}\rho'\boldsymbol{e}_z \tag{5.4b}$$

$$\frac{D\rho'}{Dt} - w\frac{d\overline{\rho}}{dz} = \frac{1}{\mathrm{PrRe}}\nabla^2(\overline{\rho} + \rho') \tag{5.4c}$$

$$\frac{D\overline{\rho}}{Dt} = 0\ . \tag{5.4d}$$

Here p' is the deviatoric pressure.

In terms of the ambient and deviatoric densities, the ambient potential energy is

$$\phi_b^* = \frac{1}{\pi_1 F^2}\overline{\rho}(z)z \tag{5.5}$$

and

$$\phi_a^* = \phi - \phi_b^* = \frac{1}{\pi_1 F^2}\rho'(\boldsymbol{x}, t)z. \tag{5.6}$$

If the fluid is inviscid then $\phi_b^* = \phi_b$ and $\phi_a^* = \phi_a$.

5.0.1 Uniform ambient density gradient

When $d\hat{\overline{\rho}}/d\hat{z}$ is constant then the characteristic length scale can be defined as

$$\hat{L} = -\frac{\hat{\rho}_0}{d\hat{\overline{\rho}}/d\hat{z}}$$

and the buoyancy frequency is

$$\hat{N} = \left(\frac{\hat{g}}{\hat{\rho}_0}\frac{d\hat{\overline{\rho}}}{d\hat{z}}\right)^{1/2}\ .$$

In terms of $\hat{N}$,

$$F^2 = \frac{\hat{V}^2}{\pi_1 \hat{N}^2 \hat{L}^2}\ .$$

Following the analysis of Holliday and McIntyre [1981] but without assuming an ideal fluid,

$$\phi_a^*(\boldsymbol{x}, t) = -\frac{1}{2\pi_1 F^2}[\rho'(\boldsymbol{x}, t)]^2 \tag{5.7}$$

which evolves in time according to

$$\frac{D\phi_a^*(\boldsymbol{x},t)}{Dt} = -\frac{\rho'(\boldsymbol{x},t)w}{F^2} + \frac{\nabla^2\rho'(\boldsymbol{x},t)}{\pi_1 \mathrm{F}^2\mathrm{PrRe}} + \epsilon_\Phi, \tag{5.8}$$

where

$$\epsilon_\Phi = \frac{\nabla\rho'(\boldsymbol{x},t)\cdot\nabla\rho'(\boldsymbol{x},t)}{\pi_1 \mathrm{F}^2\mathrm{PrRe}} \tag{5.9}$$

is the irreversible dissipation rate of ϕ_a^* due to diapycnal mixing.

5.0.2 Hyperbolic Tangent Ambient Profile

Next consider the ambient density profile

$$\hat{\overline{\rho}}(\hat{z}) = \hat{\varrho}\tanh\left(\frac{\hat{z}}{\hat{\delta}_\rho}\right) \tag{5.10}$$

where

$$\hat{\varrho} = -\frac{\Delta\hat{\overline{\rho}}}{2}\coth\left(\frac{\hat{h}}{2\hat{\delta}_\rho}\right) ,$$

$\hat{h}$ is the height of the computational domain, $\Delta\hat{\overline{\rho}}$ is the difference between the maximum and minimum values of $\hat{\overline{\rho}}$, and $\hat{\delta}_\rho$ is the characteristic height of the ambient density profile. In the limit of large $\hat{\delta}_\rho$, this profile is the same as for linear stratification provided that the dimensionless group $\hat{L}\Delta\hat{\overline{\rho}}/\hat{h}\hat{\rho}_0 = 1$. Then the average buoyancy frequency is

$$\hat{\overline{N}} = \left(-\frac{g}{\hat{\rho}_0}\frac{\Delta\hat{\overline{\rho}}}{\hat{h}}\right)^{1/2}$$

in terms of which

$$F = \left(\frac{\hat{V}^2}{\pi_1\hat{N}^2\hat{L}^2}\right)^{1/2} .$$

Following the analysis of Holliday and McIntyre [1981] but without the assumption of an ideal fluid, Hebert [2007] determined

$$\phi_a^*(\boldsymbol{x},t) = -\frac{\delta_\rho}{\pi_1 F^2}\left[\rho\,\mathrm{arctanh}\left(\frac{\varrho\rho'}{\varrho^2-\overline{\rho}\rho'-\overline{\rho}^2}\right) + \frac{\varrho}{2}\ln\left(\frac{\varrho^2-\rho^2}{\varrho^2-\overline{\rho}^2}\right)\right] . \tag{5.11}$$

For this case,

$$\epsilon_\Phi = -\frac{\delta_\rho}{\pi_1 \mathrm{F}^2 \mathrm{PrRe}} \mathrm{arctanh}\left(\frac{\varrho\rho'}{\varrho^2 - \overline{\rho}\rho' - \overline{\rho}^2}\right) \nabla^2\rho'. \tag{5.12}$$

In the preceding equations the spatial and temporal dependencies of the variables have been omitted for clarity of the notation. The relations for ϕ_a^* derived in this here are used in chapter 6 in the simulations of linear and hyperbolic tangent cases.

CHAPTER 6

DIRECT NUMERICAL SIMULATIONS

Now we illustrate the concepts developed in §1.2 and chapter 5 with two direct numerical simulations. The first configuration uses a linear ambient density profile and has been identified as F4R32 in previously published papers [Riley and de Bruyn Kops, 2003, de Bruyn Kops et al., 2003, Hebert and de Bruyn Kops, 2006a,b]. It is referred to here as the linear profile case. The second configuration has the same average ambient density gradient but a tanh ambient density profile. It is referred to as the tanh profile case. Each configuration is simulated several times with different vertical grid spacings, as detailed below.

6.1 Numerical Method

A pseudo-spectral technique is used in the simulations to solve (5.4) with the deviatoric density field initially zero everywhere and the velocity field initialized with Taylor-Green [Taylor and Green, 1937] vortices plus a small amount of white noise. The technique is discussed in detail in the papers cited in the preceding paragraph.

Briefly, the momentum equations are solved with the non-linear term in rotational form, and the fractional step approach is used to enforce non-divergence. A spherical wave-number truncation of 15/16 κ_{max} is used in order to eliminate major aliasing errors, where κ_{max} is the maximum wave number in discrete Fourier transforms. Differentiation and addition are computed in Fourier space, and multiplication is done in real space. The non-linear term in the energy equation is solved in advection

and conservation form on alternate time steps. The equations are advanced in time with the third-order, variable time step, Adams-Bashforth algorithm.

The fractional step method (also known as pressure projection method) is a two step method to solve for the velocity field. In the first step, the velocity fields are advanced in time without considering the pressure term in the momentum equation. In the second step, by using the incompressible assumption, the pressure is expressed as a Poisson equation in terms of the new velocity fields. This Poisson equation is then solved for pressure and the pressure is used to "correct" the values of the velocity fields computed in the first step. Further discussion on the fractional step method can be found in Perot [1993].

The simulation domain is a box that is periodic in all directions. Each horizontal direction has length 4π discretized with 512 grid points. The vertical dimension has length 2π discretized with 256, 512, 1024, or 2048 grid points. So the linear case with 256 vertical grid points is exactly the same configuration as case F4R32 in Table 1 of Riley and de Bruyn Kops [2003].

The dimensionless parameters for both simulations are Re = 3200, F = 4, Pr = 1, $\pi_1 = 1$, $\pi_2 = 1$, $\gamma = 1$, and $\lambda = 1$. Recall from §5.0.2 that choosing $\hat{L}\Delta\hat{\bar{\rho}}/\hat{h}\hat{\rho}_0 = 1$ results in flows with linear and tanh ambient profiles having the same Froude number if they have the same mean density gradient. The only difference in parameters between the linear and tanh configurations is that in the linear case $\delta_\rho \to \infty$ and in the tanh case $\delta_\rho = 1$ so that the characteristic height of the density profile is the same as that of the initial velocity field. The ambient density profiles are shown in Fig. 6.1. Also shown is the nominal u-velocity profile, $\cos(z)$. A three-dimensional contour plot of the initial stream function is given as Fig. 1 in Riley and de Bruyn Kops [2003].

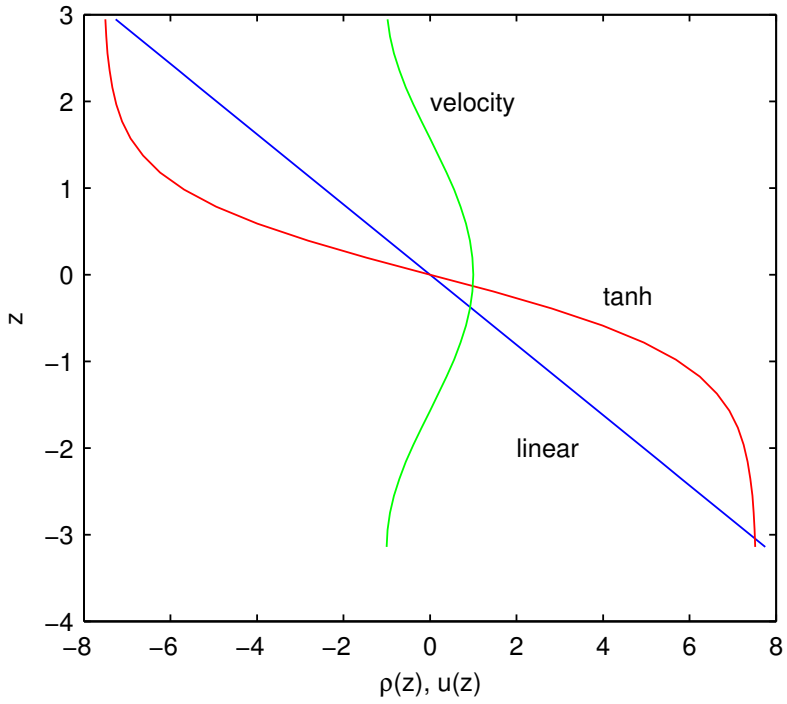

Figure 6.1. Profiles of the ambient density and nominal x-direction velocity.

6.2 Budget of Spatially-Averaged Energy

An overview of the energy budgets for both ambient density configurations is provided by Fig. 6.2 and Fig. 6.3. Included in the plots is the quantity

$$\psi(t) = K + \Phi_a^* + \int_0^t \langle \epsilon_K(\tau) \rangle + \langle \epsilon_\Phi(\tau) \rangle \, d\tau,$$

where ϵ_K is the local dissipation rate of kinetic energy. Since the simulated flows are solutions to (1.10), ψ should be constant. Not shown on the figure is the average internal energy, which is constant since under the Boussinesq approximation viscous dissipation of kinetic energy does not cause heating (c.f. (1.12b)). It is apparent kinetic, internal, and deviatoric energies balance but potential energy does not. This is a result of choosing to solve equations for mass, momentum, and thermal energy with the Boussinesq assumptions strictly enforced. If equations for, say, mass, momentum,

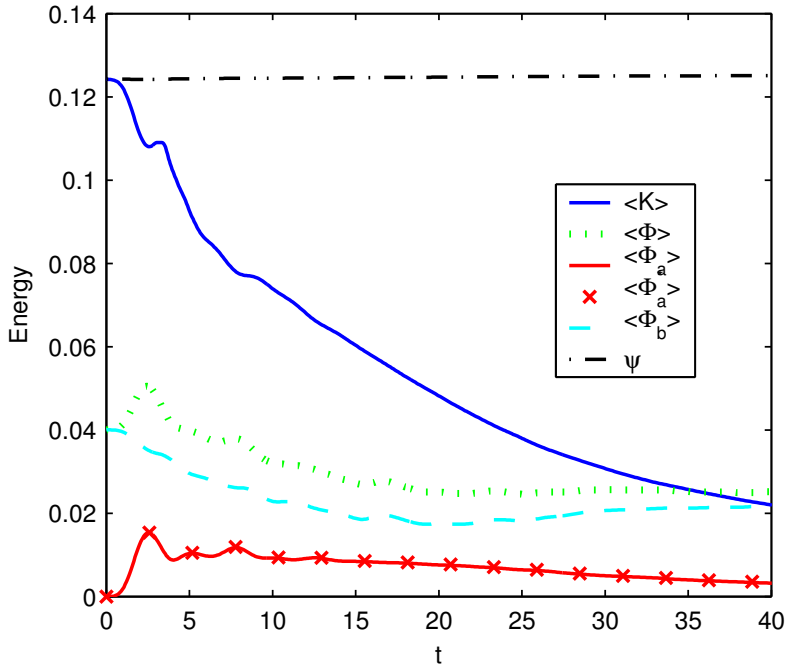

Figure 6.2. Domain-averaged energies versus time for the linear case with 512 grid points in the vertical direction.

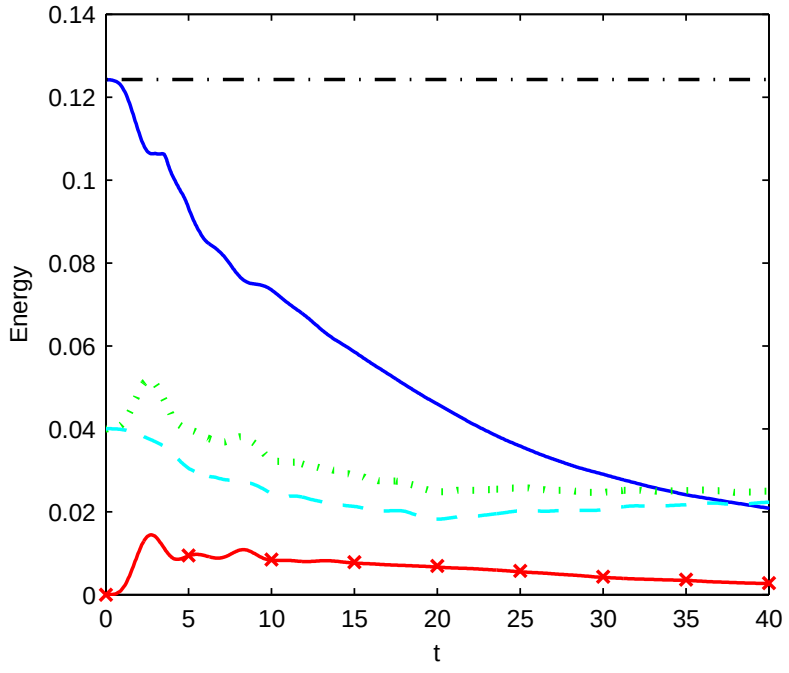

Figure 6.3. Domain-averaged energies versus time for the tanh case with 512 grid points in the vertical direction.

and potential energy were solved then the energy imbalance illustrated in Fig. 6.2 and Fig. 6.3 would be manifested in some other way.

6.3 Results

The variation in $\langle \Phi \rangle (t)$ with time in the simulations is straightforward to understand. Part of the variation is due to the use of periodic boundary conditions even though the mean density gradient is not zero. This configuration allows fluid parcels with lower density than any initially in the domain to convect in at the top boundary and, similarly, heavy fluid parcels to convect in through the bottom boundary. Additional variation in $\langle \Phi \rangle (t)$ is due to the nature of Boussinesq fluids. To see this, consider stirring of a variable-density fluid. In a real fluid, a fluid element advected upward can expand, and one advected downward can compress, so that stirring conserves potential energy via pressure work. A Boussinesq fluid parcel has constant volume, though, and so potential energy cannot be conserved.

Although background potential energy is created irreversibly, $\langle \Phi_b \rangle (t)$ does not monotonically increase in time. This behavior is due to convection through the top and bottom boundaries and also due to non-conservation of potential energy in (1.13). The results are not shown, but the simulations were run out for a very long check that $\langle \Phi_b \rangle (t)$ does asymptotically approach its initial value at late time. It is clear from the plots in figures 6.2 and 6.3 that the potential energy is not conserved. As the kinetic energy in the domain decreases over time, ideally the potential energy in the box should increase correspondingly, so that the total energy in the box is conserved. However, in the cases of both the linear and hyperbolic tangent cases, the relative error in potential energy is 84%.

6.3.1 Comparison of Available and Deviatoric Energies

In Fig. 6.2, and Fig. 6.3, $\langle \Phi_a \rangle (t)$ is shown as a line and $\langle \Phi_a^* \rangle (t)$ as symbols. It is apparent that $\langle \Phi_a^* \rangle (t)$ is a good surrogate for $\langle \Phi_a \rangle (t)$ in these simulations as averaged over the domain. Now we consider the differences in the local values Φ_a and Φ_a^*. The PDFs of each are plotted in Fig. 6.4 for linearly stratified configuration with 256, 512, 1024, and 2048 grid points in the vertical. Most striking is the jitter in $P(\Phi_a)$ due to discretization of the vertical coordinate. Therefore, the errors in available potential energy associated to descritization are evident in this plot.

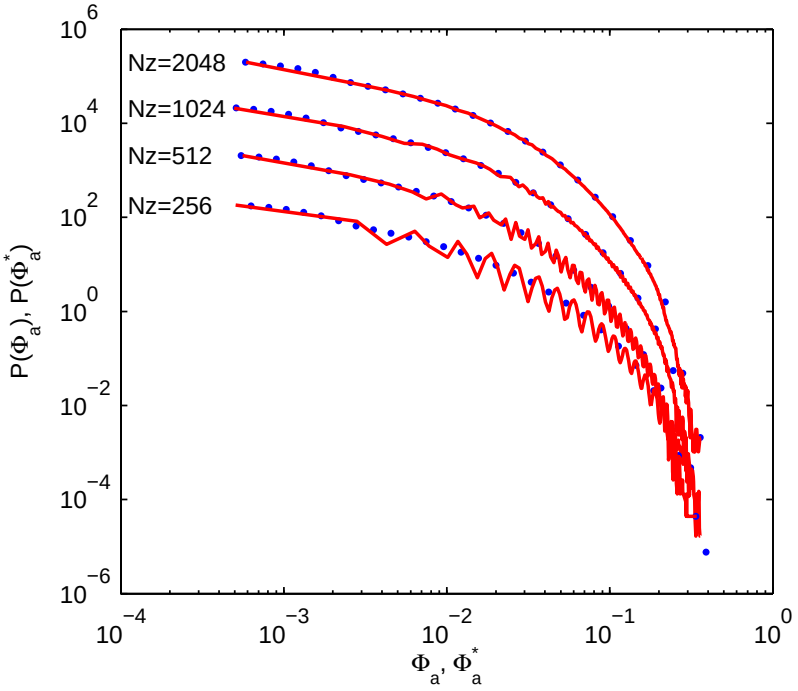

Figure 6.4. Probability densities of Φ_a (lines) and Φ_a^* (symbols) for the linear cases at $t = 10$. The case with Nz $= 256$ is plotted true and the others are offset in increments of one decade.

As noted previously, two fluid elements with identical density elevation may be assigned different values of Φ_a. The same does not happen with Φ_a^*. So $P(\Phi_a^*)$ is smooth and does not vary with the resolution of the simulations whereas $P(\Phi_a)$ requires at least 1024 grid points in the vertical in order for the PDF to converge.

Results for the tanh case are comparable. More detailed analysis of the convergence of Φ_a with grid resolution is reported by Molemaker and McWilliams [2010]. How Φ_a and Φ_a^* compare locally can be measured by the joint probability density of their common logarithms, which is shown in the Fig. 6.5 for the linear case at the highest resolution. For the vast majority of locations, $\Phi_a^* \approx \Phi_a$. At other locations the two quantities differ by orders of magnitude.

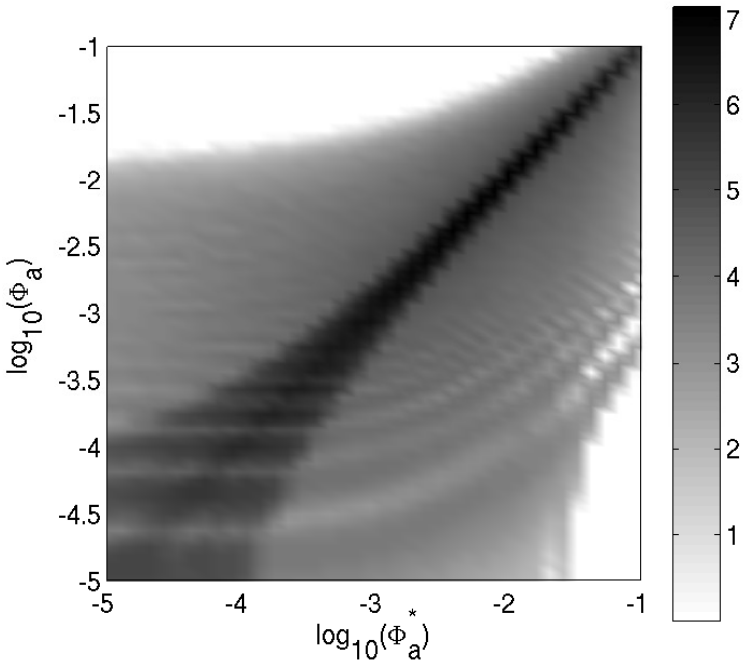

Figure 6.5. Joint PDF of $\log_{10}(\Phi_a)$ and $\log_{10}(\Phi_a^*)$ for the linear case with 2048 grid points in the vertical at $t = 10$. The shading indicates the common logarithm of the probability density.

CHAPTER 7

CONCLUSIONS AND FUTURE WORK

Lorenz's partition of potential energy into its available and background components is well established for studying the energetics of stratified flows. For a hypothetical container of fluid, both quantities are straightforward to compute. The analogous local quantities $\phi_a(\boldsymbol{x}, t)$ and $\phi_b(\boldsymbol{x}, t)$, which are necessary for computing one- and multi-point statistics of energy, can be calculated accurately only in the case wherein the density field is known analytically as shown in chapter 3. However these local quantities cannot be accurately computed numerically, because discretization of the vertical coordinate introduces significant error into the calculation. Since $\phi_a(\boldsymbol{x}, t)$ cannot be computed locally, the rate of its conversion to $\phi_b(\boldsymbol{x}, t)$ cannot be determined directly.

The foregoing conclusions apply to a real fluid. In numerical simulations the accurate computation of the local energetics is further complicated if the assumptions of Boussinesq [1903] are made. Whereas the assumptions are approximately correct for real flows under certain conditions, enforcing them literally in simulations results in significant errors in quantities that are inferred rather computed directly from transport equations. For instance, if equations for mass, momentum, and thermal energy are solved then potential energy will not be conserved. This complicates the interpretation of average available and background potential energy and raises significant questions about the meaning of the local analogs $\phi_a(\boldsymbol{x}, t)$ and $\phi_b(\boldsymbol{x}, t)$.

A possible alternative to $\phi_a(\boldsymbol{x}, t)$ and $\phi_b(\boldsymbol{x}, t)$ are the deviatoric and ambient potential energies, $\phi_a^*(\boldsymbol{x}, t)$ and $\phi_b^*(\boldsymbol{x}, t)$. Unlike the local available and background

energies, they can be computed very accurately and they are differentiable to the extent that the density field is. Furthermore, energy balances involving $\phi_a^*(\boldsymbol{x},t)$ and $\phi_b^*(\boldsymbol{x},t)$ can be closed to high precision, which is an important step in verifying that a simulation is numerically accurate.

A shortcoming of $\phi_a^*(\boldsymbol{x},t)$ and $\phi_b^*(\boldsymbol{x},t)$ is that they are not exactly equal to the quantities of theoretical interest, that is, available and background potential energies. To measure the differences between $\phi_a^*(\boldsymbol{x},t)$ and $\phi_a(\boldsymbol{x},t)$, a set of direct numerical simulations is considered that involves both linear and non-linear ambient density gradients. It is shown, as is commonly assumed, that the sum of kinetic and deviatoric potential energy accurately balance in DNS. The lack of conservation of potential energy, which is shown analytically, is verified in the simulations. Finally, $\phi_a^*(\boldsymbol{x},t)$ is shown to be a good surrogate for $\phi_a(\boldsymbol{x},t)$ in the great majority of spatial locations, although there are large differences between the two quantities at some locations. The differences are due partly to the fact that the two quantities are fundamentally different and partly do to calculations of $\phi_a(\boldsymbol{x},t)$ suffering from large errors due to discretization of the vertical coordinate.

The results suggest that deviatoric and ambient potential energies are likely to be useful for understanding the energetics of stratified flows. There are differences between them and the theoretical quantities introduced by Lorenz, but since simulations in which the Boussinesq assumptions are made do not conserve mass or energy locally, and since the calculation of available potential energy is strongly subject to discretization errors, the difference between deviatoric and available energies is likely small compared with other limitations of simulations.

7.1 Summary

In the mathematical models used to simulate buoyancy driven stratified flows, Boussinesq approximations are widely used to simplify the governing equations. The

equation of state, derived by ignoring isothermal compressibility of the fluid, leads to significant discrepancies in the transport equations for energy for a localized fluid parcel. The full governing equations for a Boussinesq fluid are derived rigorously in this thesis. Following a series expansion approach, the terms that can be computed in a numerical simulation are identified and listed in the implied energy equations (§1.2.3). Various terms in the implied energy equations are identified and analyzed using the analytical approach for both, a rigid adiabatic control volume and a one that allows mass transfer at the boundaries. The implied energy equations and the corresponding analytical solution confirm that Boussinesq approximations are not energy conserving. Moreover, only when the condition $F^2 = \pi_2$ is satisfied, is the potential energy in a Boussinesq fluid is conserved.

In the Boussinesq model, partitioning of potential energy into available and background potential energy locally becomes even more difficult. This is primarily due to the errors introduced by the Boussinesq equation of state in the diffusion term of transport equation for potential energy. Moreover, local available potential energy, by definition, is sensitive to descritization errors. The only way to compute a potential energy balance locally, independent of descritization errors in by computing analytical functions for energies as shown in chapter 3. But this approach is limited to very few 1-D cases, in which the continuity equation can be solved analytically inside a periodic domain. In this thesis we have used the stochastic approach of Tseng and Ferziger [2001] to develop a method to numerically compute available potential energy locally. By comparison with analytical solutions we have shown the numerical computation to be highly accurate of 1-D cases.

In a 3-D domain, however, a fluid parcel with a certain value of available potential energy can be located at either of at least two vertical locations separated by Δz. In other words, by traditional definition, local available potential energy is sensitive to

descritization errors. These errors, coupled with Boussinesq approximations lead to the potential energy is not being conserved locally.

In this thesis we have introduced ambient and deviatoric potential energy as surrogates for available and background potential energies. Direct Numerical Simulations, known for their high resolution in space and time, are used to simulate the Boussinesq fluid, with both linear and hyperbolic tangent density profiles. In both cases, deviatoric energies balance exactly when averaged over the domain. Locally, deviatoric energy matches the available potential energy at majority of spatial locations, as shown in results. Also, since there is possibility that available potential energy might be erroneous at certain locations, the deviatoric potential energy proves to be an attractive surrogate. Overall, ambient and deviatoric potential energy are a useful tool in formulating an energy budget for stratified fluids.

The mathematical framework for modeling Boussinesq fluids developed in this thesis has been maintained to the most generalized form. Applications of this model to compute local potential energy balances in variety of flow conditions is part of prospective work on this topic. How the surrogate quantities perform in particular settings is an area of further research.

APPENDIX

VOLUMETRIC EVOLUTION EQUATIONS FOR POTENTIAL ENERGY

Here we derive the equations for evolution of potential energy for an arbitrary volume, by integrating implied energy equations (2.10) over z for 1-D case (listed below for reference).

$$\frac{D\Phi}{Dt} = -\frac{z\nabla^2\theta}{\mathrm{Pr\ Re\ F^2}} - \frac{\theta w}{\mathrm{F^2}}, \tag{A.1a}$$

$$\frac{D\Phi_b}{Dt} = -\frac{Z_*\nabla^2\theta}{\mathrm{Pr\ Re\ F^2}}, \tag{A.1b}$$

$$\frac{D\Phi_a}{Dt} = -\frac{z\nabla^2\theta}{\mathrm{Pr\ Re\ F^2}} + \frac{Z_*\nabla^2\theta}{\mathrm{Pr\ Re\ F^2}} - \frac{\theta w}{\mathrm{F^2}}\ . \tag{A.1c}$$

By integrating the evolution equations for energy, we can use the divergence theorem to evaluate surface integrals and characterize energy changes as surface fluxes or exchange with other forms of energy. The first term on the left hand side of (A.1a) can be expanded as $z\nabla^2\theta = \nabla\cdot(z\nabla\theta) - \nabla\cdot(\theta\nabla z)$. The equations derived are as follows:

$$\int_V \frac{DE_p}{Dt} = -\frac{1}{\mathrm{Re\ Pr\ F^2}}\oint_S z\nabla\theta\cdot\bar{n}\,dS + \frac{1}{\mathrm{Re\ Pr\ F^2}}\oint_S \theta\nabla z\cdot\bar{n}\,dS + \underbrace{\int_V \frac{w}{\pi_1\mathrm{F^2}}\left(1-\pi_1\,\theta\right)\right)\,dV}_{\phi_z}. \tag{A.2}$$

The first and third terms on the right hand side of (A.2) account for the changes in TPE due to diffusive heat and mass flux and reversible exchange with kinetic energy via buoyancy respectively. The second term, however, arises from the Boussinesq equation of state (1.4) and gives the rate of change of TPE due to exchange with internal energy.

Evolution equation for background potential energy can be derived by using (1.4), (2.4) and by definition of background potential energy, $\Phi_b = \rho Z_*/\pi_1 \mathrm{F}^2$. Again we expand the divergence term keeping in mind that $\nabla z_* = (dz_*/d\theta)\ \nabla\theta$.

$$\int_V \frac{DE_b}{Dt} = \underbrace{-\frac{1}{\mathrm{Re\ Pr\ F^2}} \oint_S z_* \nabla\theta \cdot \bar{n}\, dS}_{S_{diff}} + \underbrace{\frac{1}{\mathrm{Re\ Pr\ F^2}} \int_V -\frac{dz_*}{d\theta} |\nabla\theta|^2\, dV}_{\phi_d} \qquad \text{(A.3)}$$

The first term on the right hand side of (A.3) accounts for change in BPE due to diffusive heat and mass fluxes across the bounding surface S, while the second term gives the change in BPE due to material changes in density in the volume V. In case of a close system, $S_{diff} = 0$.

Evolution equation for available potential energy for a volume can be derived by following the approach in chapter 2, $\Phi_a = \Phi - \Phi_b$.

$$\int_V \frac{DE_a}{Dt} = -\frac{1}{\mathrm{Re\ Pr\ F^2}} \oint_S (z - z_*)\ \nabla\theta \cdot \bar{n}\, dS + \oint_S \theta\ \nabla z \cdot \bar{n}\, dS + \phi_z - \phi_d\ . \qquad \text{(A.4)}$$

Equations (A.2), (A.3) and (A.4) are used to plot energy balances in Figures 3.2 and 3.5 in the analytical examples in chapter 3.

BIBLIOGRAPHY

J. Boussinesq. *Théorie analytique de la chaleur*, volume 2, p. 172. Gauthier-Villars, Paris, 1903.

E. A. Spiegel and G. Veronis. On the Boussinesq approximation for a compressible fluid. *Astrophys J.*, 131:442–447, 1960.

E. N. Lorenz. Available potential energy and the maintenance of the general circulation. *Tellus*, 7:157–167, 1955.

D. Holliday and M. McIntyre. On potential energy density in an incompressible, stratified fluid. *J. Fluid Mech.*, 107:221–225, 1981.

Ronald L. Panton. *Incompressible Flow*. John Wiley and Sons, 2nd edition, 1996.

L. Xu, S. Raman, and Mandala R. V. A review of non-hydrostatic numerical methods for the atmoshphere. *World Congress of Nonlinear Analysts 1992 proceedings*, 4: 3595–3609, 1992.

S. Klainerman and A. Majda. Compressible and incompressible fluids. *Commun. Pur. Appl. Math.*, 35:629–651, 1982.

A. W. Cook and J. J. Riley. Direct numerical simulation of a turbulent reactive plume on a parallel computer. *J. Comput. Phys.*, 129:263–283, 1996.

P. A. McMurtry, W.-H. Jou, J. J. Riley, and R. W. Metcalfe. Direct numerical simulations of a reacting mixing layer with chemical heat release. *AIAA J.*, 24:962, 1986.

Y. Jang and S. M. de Bruyn Kops. Pseudo-spectral numerical simulation of miscible fluids with a high density ratio. *Comput. Fluids*, 36:238–247, 2007.

R. Byron Bird, Warren E. Stewart, and Edwin N. Lightfoot. *Transport Phenomena*. Wiley, New York, second edition, 2002.

Y. Ogura and N. A. Phillips. Scale analysis of deep and shallow convection in the atmosphere. *Journal of Atmospheric Sciences*, 19:173–179, 1961.

J. M. Mihaljan. A rigorous exposition of Boussinesq approximations applicable to a thin layer of fluid. *Astrophys. J.*, 136(3):1126–1133, 1962.

K. B. Winters, P. N. Lombard, J. J. Riley, and E. A. D'Asaro. Available potential energy and mixing in density-stratified fluids. *J. Fluid Mech.*, 289:115–128, 1995.

Yu-heng Tseng and J. H. Ferziger. Mixing and available potential energy in stratified flows. *Phys. Fluids*, 13(5):1281–1293, 2001.

S. B. Pope. *Turbulent Flows*. Cambridge University Press, Cambridge, 2000.

Papoulis. *Probability, Random Variables, and Stochastic Processes*. McGraw Hill Inc., 1965.

D. A. Hebert. *Mixing in stably stratified flows*. PhD thesis, University of Massachusetts Amherst, 2007.

J. J. Riley and S. M. de Bruyn Kops. Dynamics of turbulence strongly influenced by buoyancy. *Phys. of Fluids*, 15(7):2047–2059, 2003.

S. M. de Bruyn Kops, J. J. Riley, and K. B. Winters. Reynolds and Froude number scaling in stably-stratified flows. In *Reynolds Number Scaling in Turbulent Flow*. Kluwer, 2003.

D. A. Hebert and S. M. de Bruyn Kops. Relationship between vertical shear rate and kinetic energy dissipation rate in stably stratified flows. *Geophys. Res. Let.*, 33: L06602, 2006a. doi:10.1029/2005GL025071.

D. A. Hebert and S. M. de Bruyn Kops. Predicting turbulence in flows with strong stable stratification. *Phys. Fluids*, 18(6):1–10, 2006b.

G. I. Taylor and A. E. Green. Mechanism of the production of small eddies from large ones. *P. Roy. Soc. Lond. A. Mat.*, 158:499–521, 1937.

J. B. Perot. An analysis of the fractional step method. *J. Comput. Phys.*, 108:51–58, 1993.

M. Jeroen Molemaker and James C. McWilliams. Local balance and cross-scale flux of available potential energy. *J. Fluid Mech.*, 645:295–314, 2010.